

Sensor-Based Reactive Navigation in Convex Sphere Worlds

Omur Arslan and Daniel E. Koditschek

Abstract—We construct a sensor-based feedback law that solves the real-time collision free robot navigation problem in a compact convex Euclidean subset cluttered with separated and strongly convex obstacles. Our algorithm introduces a novel use of separating hyperplanes for identifying the robot’s local obstacle free convex neighborhood, affording a piecewise smooth continuously varied closed loop vector field whose smooth flow brings almost all configurations in the robot’s free space to a designated goal location, with the guarantee of no collisions along the way. We extend these provable properties to practically motivated limited range sensing models, and the nonholonomically constrained kinematics of the standard differential drive vehicle.

I. INTRODUCTION

Agile navigation in dense human crowds [22, 50], or in natural forests, such as now negotiated by rapid flying [26, 41] and legged [25, 52] robots, strongly motivates the development of sensor-based reactive motion planners. By the term *reactive* [12, 34] we mean that motion is generated by a vector field arising from some closed loop feedback policy issuing force or velocity commands in real time as a function of instantaneous state. By the term *sensor-based* we mean that information about the location of the environmental clutter to be avoided is limited to structure perceived within some local neighborhood of the robot’s instantaneous position — its sensor footprint.

In this paper, we propose a new reactive motion planner taking the form of a feedback law for a first-order (velocity-controlled), perfectly sensed and actuated disk robot, relative to a fixed goal location, that can be computed using only information about the robot’s instantaneous position and structure within its sensor footprint. We assume the a priori unknown environment is a static topological sphere world [30], whose obstacles are convex and have smooth boundaries whose curvature is “reasonably” high relative to their mutual separation. Under these assumptions, the proposed closed loop vector field is guaranteed to bring almost all initial conditions to the desired goal. To the best of our knowledge, this is the first time a sensor-based reactive motion planner has been shown to be provably correct w.r.t. a general class of environments.

A. Motivation and Prior Literature on Vector Field Planners

The simple, computationally efficient artificial potential field approach to real-time obstacle avoidance [28] incurs topologically necessary critical points [29], which, in practice, with no further remediation often include (topologically unnecessary) spurious local minima. Even in topologically simple settings such as the sphere worlds addressed here, constructions that eliminate these spurious attractors — e.g.,

The authors are with the Department of Electrical and Systems Engineering, University of Pennsylvania, Philadelphia, PA 19104, USA. E-mail: {omur, kod}@seas.upenn.edu. This work was supported by AFOSR under the CHASE MURI FA9550-10-1-0567.

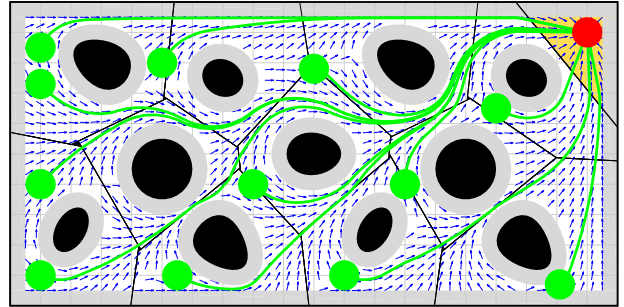


Fig. 1. Exact navigation of a disk-shaped robot using separating hyperplanes of the robot body (red at the goal) and convex obstacles (black solid shapes). Separating hyperplanes between the robot and obstacles define an obstacle free convex neighborhood (the yellow region when the robot at the goal) of the robot, and the continuous feedback motion towards the metric projection of a given desired goal (red) onto this convex set asymptotically steers almost all robot configurations (green) to the goal without collisions along the way. The grey regions represent the augmented workspace boundary and obstacles, and the arrows show the direction of the resulting vector field.

navigation functions [45], or other methods [15] — have largely come at the price of complete prior information.

Extensions to the navigation function framework partially overcoming the necessity of global prior knowledge of (and consequent parameter tuning for) a topologically and metrically simple environment have appeared in the last decade [18, 35]. Sequential composition [9] has been used to cover metrically complicated environments with convex cell-based local potential decompositions [13] (and extended to non-holonomically constrained finite size robots [14]), but still necessitating prior global knowledge of the environment.

B. Contributions and Organization of the Paper

This paper abandons the smooth potential field approach to reactive planning, achieving an algorithm that is “doubly reactive” in the sense that not merely the integrated robot trajectory, but also its generating vector field can be constructed on the fly in real time using only local knowledge of the environment. Our piecewise smooth vector field combines some of the ideas of sensor-based exploration [11] with those of hybrid reactive control [13]. We use separating hyperplanes of convex bodies [6] to identify an obstacle free convex neighborhood of a robot configuration, and build our safe robot navigation field by control action towards the metric projection of the designated point destination onto this convex set.¹

¹ In prior work [2], a different construction based on power diagrams [4] is proposed for navigating among spherical obstacles using knowledge of Voronoi-adjacent¹⁰ obstacles to construct the robot’s local workspace [2, Eqn. (9)]. This paper introduces a new construction for that set in (7) based on separating hyperplanes, permitting an extension of the navigable obstacles to the broader class of convex bodies specified by Assumption 2, while providing the same guarantee of almost global asymptotic convergence (Theorem 3) to a given goal location. From the view of applications, the new appeal to separating hyperplanes permits the central advance of a purely reactive construction from limited range sensors (23), e.g., in the planar case from immediate line-of-sight appearance (29), with the same global guarantees.

Our construction requires no parameter tuning and requires only local knowledge of the environment in the sense that the robot needs only locate those proximal obstacles determining its collision free convex neighborhood. When the obstacles are sufficiently separated (Assumption 1 stipulates that the robot must be able to pass in between them) and sufficiently strongly convex at their “antipode” (Assumption 2 stipulates that they curve away from the enclosing sphere centered at the destination which just touches their boundary at the most distant point), the proposed vector field generates a smooth flow with a unique attractor at the specified goal location along with (the topologically necessary number of) saddles — at least one associated with each obstacle. Since all of its critical points are nondegenerate, our vector field is guaranteed to steer almost all collision free robot configurations to the goal, while avoiding collisions along the way, as illustrated in Fig. 1.

It proves most convenient to develop the theoretical properties of this construction under the assumption that the robot can identify and locate those nearby obstacles whose associated separating hyperplanes define the robot’s obstacle free convex neighborhood (a capability termed *Voronoi-adjacent obstacle sensing* in Section III-B). Thus, to accommodate more physically realistic sensors, we adapt the initial construction (and the proof) to the case of two different limited range sensing modalities. Similarly, in the interest of greater practicability we further extend the construction (and the proof) to the case of the commonly encountered kinematic differential drive vehicle model (retaining the convergence and collision avoidance guarantees, at the necessary cost of a discontinuous feedback law).

This paper is organized as follows. Section II continues with a formal statement of the problem at hand. Section III briefly summarizes a separating hyperplane theorem of convex bodies, and introduces its use for identifying collision free robot configurations. Section IV, comprising the central contribution of the paper, constructs and analyzes the reactive vector field planner for safe robot navigation in a convex sphere world, and provides its more practical extensions. Section V illustrates the qualitative properties of the proposed vector field planner using numerical simulations. Section VI concludes with a summary of our contributions and a brief discussion of future work.

II. PROBLEM FORMULATION

Consider a disk-shaped robot, of radius $r \in \mathbb{R}_{>0}$ centered at $x \in \mathcal{W}$, operating in a closed compact convex environment \mathcal{W} in the n -dimensional Euclidean space \mathbb{R}^n , where $n \geq 2$, punctured with $m \in \mathbb{N}$ open convex sets $\mathcal{O} := \{O_1, O_2, \dots, O_m\}$ with twice differentiable boundaries, representing obstacles.² Hence, the free space \mathcal{F} of the robot is given by

$$\mathcal{F} := \left\{ x \in \mathcal{W} \mid \overline{B(x, r)} \subseteq \mathcal{W} \setminus \bigcup_{i=1}^m O_i \right\}. \quad (1)$$

where $B(x, r) := \{q \in \mathbb{R}^n \mid \|q - x\| < r\}$ is the open ball centered at x with radius r , and $\overline{B(x, r)}$ denotes its closure, and $\|\cdot\|$ denotes the standard Euclidean norm.

² Here, \mathbb{N} is the set of all natural numbers; \mathbb{R} and $\mathbb{R}_{>0}$ ($\mathbb{R}_{\geq 0}$) denote the set of real and positive (nonnegative) real numbers, respectively.

³ Assumption 1 is equivalent to the “isolated” obstacles assumption of [45].

To maintain the local convexity of obstacle boundaries in the free space \mathcal{F} , we assume that our disk-shaped robot can freely fit in between (and thus freely circumnavigate) any of the obstacles throughout the workspace \mathcal{W} :³

Assumption 1 *Obstacles are separated from each other by clearance of at least $d(O_i, O_j) > 2r$ for all $i \neq j$, and from the boundary $\partial\mathcal{W}$ of the workspace \mathcal{W} as $d(O_i, \partial\mathcal{W}) > 2r$ for all $i = 1 \dots m$, where $d(A, B) := \inf\{\|a - b\| \mid a \in A, b \in B\}$.*

Before formally stating our navigation problem, it is useful to recall the well known topological limitation of reactive planners: if a continuous vector field planner on a generalized sphere world has a unique attractor, then it must have at least as many saddles as obstacles [30]. In consequence, the robot navigation problem that we seek to solve is stated as:

Reactive Navigation Problem. *Assuming the first order (completely actuated single integrator) robot dynamics,*

$$\dot{x} = u(x), \quad (2)$$

find a Lipschitz continuous controller, $u : \mathcal{F} \rightarrow \mathbb{R}^n$, that leaves the robot’s free space \mathcal{F} positively invariant and asymptotically steers almost all configurations in \mathcal{F} to any given goal $x^ \in \mathcal{F}$.*

III. ENCODING COLLISIONS VIA SEPARATING HYPERPLANES

A. Separating Hyperplane Theorem

A fundamental theorem of convex sets states that any two disjoint convex sets can be separated by a hyperplane such that they lie on opposite sides of this hyperplane:

Theorem 1 (Separating Hyperplane Theorem [6, 51]) *For any two nonintersecting convex sets $A, B \in \mathbb{R}^n$ (i.e., $A \cap B = \emptyset$), there exists $a \in \mathbb{R}^n$ and $b \in \mathbb{R}$ such that $a^T x \geq b$ for all $x \in A$ and $a^T x \leq b$ for all $x \in B$.*

For example, a usual choice of such a hyperplane is [6]:

Definition 1 *The maximum margin separating hyperplane of any two disjoint convex sets $A, B \subset \mathbb{R}^n$, with $d(A, B) > 0$, is defined to be*

$$H(A, B) := \left\{ x \in \mathbb{R}^n \mid \|x - a\| = \|x - b\|, \|a - b\| = d(A, B), a \in \overline{A}, b \in \overline{B} \right\}, \quad (3)$$

where $d(x, H(A, B)) \geq \frac{d(A, B)}{2}$ for all $x \in A \cup B$.

Another useful tool for finding a separating hyperplane between a point and a convex set is metric projection:

Theorem 2 ([51]) *Let $A \subset \mathbb{R}^n$ be a closed convex set and $x \in \mathbb{R}^n$. Then there exists a unique point $a^* \in A$ such that*

$$a^* = \Pi_A(x) := \arg \min_{a \in A} \|a - x\|, \quad (4)$$

and one has $(x - \Pi_A(x))^T (\Pi_A(x) - a) \geq 0$ for all $a \in A$. The map $\Pi_A(x)$ is called the metric projection of x onto set A .

Lemma 1 *The maximum margin separating hyperplane of a convex set $A \subset \mathbb{R}^n$ and the ball $B(x, r)$ of radius $r \in \mathbb{R}_{>0}$ centered at $x \in \mathbb{R}^n$, satisfying $d(x, A) \geq r$, is given by*

$$H(A, B(x, r)) = \left\{ y \in \mathbb{R}^n \mid \left\| y - \left(\Pi_{\overline{B(x, r)}} \circ \Pi_A \right)(x) \right\| = \|y - \Pi_A(x)\| \right\}, \quad (5)$$

where $\left(\Pi_{\overline{B(x, r)}} \circ \Pi_A \right)(x) = x - r \frac{x - \Pi_A(x)}{\|x - \Pi_A(x)\|}$.

Proof: See Appendix I-A. ■

A common application of separating hyperplanes of a set of convex bodies is to discover their organizational structure. For instance, to model its topological structure, we define the generalized Voronoi diagrams $\mathcal{V} = \{V_1, V_2, \dots, V_m\}$ of a convex environment \mathcal{W} in \mathbb{R}^n populated with disjoint convex obstacles $\mathcal{O} = \{O_1, O_2, \dots, O_m\}$ (i.e., $d(O_i, O_j) > 0 \forall i \neq j$), based on maximum margin separating hyperplanes, to be^{4 5}

$$V_i := \left\{ q \in \mathcal{W} \mid \begin{aligned} & \|q - p_i\| \leq \|q - p_j\|, \|p_i - p_j\| = d(O_i, O_j), \\ & p_i \in \overline{O_i}, p_j \in \overline{O_j} \quad \forall j \neq i \end{aligned} \right\}, \quad (6)$$

which yields a convex cell decomposition of a subset of \mathcal{W} such that, by construction, each obstacle is contained in its Voronoi cell, i.e., $O_i \subset V_i$, see Fig. 2. Note that for point obstacles, say $O_i = \{p_i\}$ for some $p_i \in \mathbb{R}^n$, the generalized Voronoi diagram of \mathcal{W} in (6) simplifies back to the standard Voronoi diagram of \mathcal{W} , generated by points $\{p_1, \dots, p_m\}$ [40].

B. The Safe Neighborhood of a Disk-Shaped Robot

Throughout the sequel, we consider a disk-shaped robot, centered at $x \in \mathcal{W}$ with radius $r \in \mathbb{R}_{>0}$, moving in a closed compact convex environment $\mathcal{W} \subseteq \mathbb{R}^n$ populated with open convex obstacles, $\mathcal{O} = \{O_1, O_2, \dots, O_m\}$, satisfying Assumption 1. Since the workspace, obstacles, and the robot radius are fixed, we suppress all mention of the associated terms wherever convenient, in order to simplify the notation.

Using the robot body and obstacles as generators of a generalized Voronoi diagram of \mathcal{W} , we define the robot's *local workspace*, $\mathcal{LW}(x)$, illustrated in Fig. 2(left), as,⁶

$$\mathcal{LW}(x) := \left\{ q \in \mathcal{W} \mid \left\| q - x + r \frac{x - \Pi_{\overline{O_i}}(x)}{\|x - \Pi_{\overline{O_i}}(x)\|} \right\| \leq \|q - \Pi_{\overline{O_i}}(x)\|, \forall i \right\}. \quad (7)$$

Note that we here take the advantage of having a disk-shaped robot and construct the maximum margin separating hyperplane between the robot and each obstacle using the robot's centroid (Lemma 1).

A critical property of the local workspace \mathcal{LW} is:

Proposition 1 *A robot placement $x \in \mathcal{W} \setminus \bigcup_{i=1}^m O_i$ is collision free, i.e., $x \in \mathcal{F}$, if and only if the robot body is contained in its local workspace $\mathcal{LW}(x)$, i.e.,⁷*

$$x \in \mathcal{F} \iff \overline{B(x, r)} \subseteq \mathcal{LW}(x). \quad (8)$$

Proof: See Appendix I-B. ■

Accordingly, we define the robot's *local free space*, $\mathcal{LF}(x)$, by eroding $\mathcal{LW}(x)$, removing the volume swept along its

⁴Generalized Voronoi diagrams and cell decomposition methods are traditionally encountered in the design of roadmap methods [11, 34, 39]. A major distinction between our construction and these roadmap algorithms is that the latter typically seek a global, one-dimensional graphical representation of a robot's environment (independent of any specific configuration), whereas our approach uses the local open interior cells of the robot-centric Voronoi diagram to determine a locally safe neighborhood of a given free configuration.

⁵It seems worth noting that our use of generalized Voronoi diagrams is motivated by another application of Voronoi diagrams in robotics for coverage control of distributed mobile sensor networks [1, 16, 33, 44].

⁶Here, to solve the indeterminacy, we set $\frac{x}{\|x\|} = 0$ whenever $x = 0$.

⁷Note that $\mathcal{F} \subsetneq \mathcal{W} \setminus \bigcup_{i=1}^m O_i$ for a disk-shaped robot of radius $r > 0$.

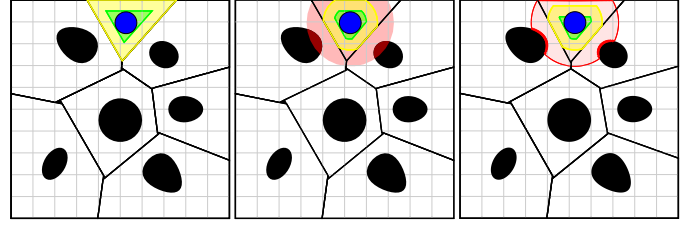


Fig. 2. Local workspace \mathcal{LW} (yellow) and local free space \mathcal{LF} (green) of a disk-shaped robot (blue) for different sensing modalities: (left) Voronoi-adjacent¹⁰ obstacle sensing, (middle) a fixed radius sensory footprint (red), (right) a limited range line-of-sight sensor (red). The boundary of each generalized Voronoi cell is defined by the maximum margin separating hyperplanes of the robot body (blue) and obstacles (black).

boundary, $\partial\mathcal{LW}(x)$, by the robot body radius, illustrated on the left in Fig. 2, as [21]⁸

$$\mathcal{LF}(x) := \mathcal{LW}(x) \setminus (\partial\mathcal{LW}(x) \oplus B(\mathbf{0}, r)), \quad (9a)$$

$$= \left\{ q \in \mathcal{LW}(x) \mid \overline{B(q, r)} \subseteq \mathcal{LW}(x) \right\}. \quad (9b)$$

Note that, for any $x \in \mathcal{F}$, $\mathcal{LF}(x)$ is a nonempty closed convex set, because $x \in \mathcal{LF}(x)$ and the erosion of a closed convex set by an open ball is a closed convex set.⁹

An immediate consequence of Proposition 1 is:

Corollary 1 *Any robot placement in the local free space $\mathcal{LF}(x)$ of a collision free robot location $x \in \mathcal{F}$ is also collision free, i.e., $\mathcal{LF}(x) \subseteq \mathcal{F}$ for all $x \in \mathcal{F}$.*

Finally, it is useful to emphasize that to construct its local workspace, the robot requires only local knowledge of the environment in the sense that the robot only needs to locate proximal obstacles — those whose Voronoi cells are adjacent¹⁰ to the robot's (local workspace). This can be achieved by assuming an adjustable radius sensory footprint and gradually increasing its sensing range until the set of obstacles in the sensing range satisfies a certain geometric criterion guaranteeing that the detected obstacles exactly define the robot's local workspace [16]. We will refer to this sensing model as *Voronoi-adjacent obstacle sensing*.

IV. ROBOT NAVIGATION VIA SEPARATING HYPERPLANES

In this section, first assuming Voronoi-adjacent obstacle sensing, we introduce a new provably correct vector field controller for safe robot navigation in a convex sphere world, and list its important qualitative properties. Then we present its extensions for two more realistic sensor models (illustrated, respectively, in the middle and the right panels of Fig. 2): a fixed radius sensory footprint and a limited range line-of-sight sensor. We further adapt our construction to the widely used nonholonomically constrained differential drive vehicle.

⁸Here, $\mathbf{0}$ is a vector of all zeros with the appropriate size, and $A \oplus B$ denotes the Minkowski sum of sets A and B defined as $A \oplus B = \{a + b \mid a \in A, b \in B\}$.

⁹The erosion of a closed half-space by an open ball is a closed half-space. Hence, since the erosion operation is distributed over set intersection [21], and a closed convex set can be defined as (possibly infinite) intersection of closed half-spaces [6], and an arbitrary intersection of closed sets is closed [38], the erosion of a closed convex set by an open ball is a closed convex set.

¹⁰A pair of Voronoi cells in \mathbb{R}^n is said to be *adjacent* if they share a $n - 1$ dimensional face.

A. Feedback Robot Motion Planner

Assuming the fully-actuated single-integrator robot dynamics in (2), for a choice of a desired goal location $x^* \in \mathcal{F}$, we propose a robot navigation strategy, called the “move-to-projected-goal” law, $u : \mathcal{F} \rightarrow \mathbb{R}^n$ that steers the robot at location $x \in \mathcal{F}$ towards the global goal x^* through the “projected goal”, $\Pi_{\mathcal{L}\mathcal{F}(x)}(x^*)$, as follows:¹¹

$$u(x) = -k(x - \Pi_{\mathcal{L}\mathcal{F}(x)}(x^*)), \quad (10)$$

where $k \in \mathbb{R}_{>0}$ is a fixed control gain and Π_A (4) is the metric projection onto a closed convex set $A \subset \mathbb{R}^n$, and $\mathcal{L}\mathcal{F}(x)$ is continuously updated using the Voronoi-adjacent obstacle sensing and its relation with $\mathcal{L}\mathcal{W}(x)$ in (9).

B. Qualitative Properties

Proposition 2 *The “move-to-projected-goal” law in (10) is piecewise continuously differentiable.*

Proof: An important property of generalized Voronoi diagrams in (6) inherited from the standard Voronoi diagrams of point generators is that the boundary of each Voronoi cell is a piecewise continuously differentiable function of generator locations [8, 46]. In particular, for any $x \in \mathcal{F}$ the boundary of the robot’s local workspace $\mathcal{L}\mathcal{W}(x)$ is piecewise continuously differentiable since it is defined by the boundary of the workspace and separating hyperplanes between the robot and obstacles, parametrized by x and $\Pi_{\overline{O}_i}(x)$, and metric projections onto convex cells are piecewise continuously differentiable [32]. Hence, the boundary of the local free space $\mathcal{L}\mathcal{F}(x)$ is also piecewise continuously differentiable because $\mathcal{L}\mathcal{F}(x)$ is the nonempty erosion of $\mathcal{L}\mathcal{W}(x)$ by a fixed open ball. Therefore, one can conclude using the sensitivity analysis of metric projections onto moving convex sets [36, 47] that the “move-to-projected-goal” law is Lipschitz continuous and piecewise continuously differentiable. ■

Proposition 3 *The robot’s free space \mathcal{F} in (1) is positively invariant under the “move-to-projected” law (10).*

Proof: Since x and $\Pi_{\mathcal{L}\mathcal{F}(x)}(x^*)$ are both in $\mathcal{L}\mathcal{F}(x)$ for any $x \in \mathcal{F}$, and $\mathcal{L}\mathcal{F}(x)$ is an obstacle free convex neighborhood of x (Corollary 1), the line segment joining x and $\Pi_{\mathcal{L}\mathcal{F}(x)}(x^*)$ is free of collisions. Hence, at the boundary of \mathcal{F} , the robot under the “move-to-projected-goal” law either stays on the boundary or moves towards the interior of \mathcal{F} , but never crosses the boundary, and so the result follows. ■

Proposition 4 *For any initial $x \in \mathcal{F}$, the “move-to-projected-goal” law (10) has a unique continuously differentiable flow in \mathcal{F} (1) defined for all future time.*

¹¹In general, the metric projection of a point onto a convex set can be efficiently computed using a standard convex programming solver [6]. If \mathcal{W} is a convex polytope, then the robot’s local free space, $\mathcal{L}\mathcal{F}(x)$, is also a convex polytope and can be written as a finite intersection of half-spaces. Hence, the metric projection onto a convex polytope can be recast as quadratic programming and can be solved in polynomial time [31]. In the case of a convex polygonal environment, $\mathcal{L}\mathcal{F}(x)$ is a convex polygon and the metric projection onto a convex polygon can be solved analytically because the solution lies on one of its edges, unless the input point is inside the polygon.

Proof: The existence, uniqueness and continuous differentiability of its flow follow from the Lipschitz continuity of the “move-to-projected-goal” law in its compact domain \mathcal{F} since a piecewise continuously differentiable function is locally Lipschitz on its domain [10], and a locally Lipschitz function on a compact set is globally Lipschitz on that set [27]. ■

Proposition 5 *The set of stationary points of the “move-to-projected-goal” law (10) is $\{x^*\} \cup \bigcup_{i=1}^m \mathfrak{S}_i$, where*

$$\mathfrak{S}_i := \left\{ x \in \mathcal{F} \mid d(x, O_i) = r, \frac{(x - \Pi_{\overline{O}_i}(x))^T (x - x^*)}{\|x - \Pi_{\overline{O}_i}(x)\| \|x - x^*\|} = 1 \right\}. \quad (11)$$

Proof: It follows from (4) that the goal location x^* is a stationary point of (10), because $x^* \in \mathcal{L}\mathcal{F}(x^*)$. In fact, for any $x \in \mathcal{F}$, one has $\Pi_{\mathcal{L}\mathcal{F}(x)}(x^*) = x^*$ whenever $x^* \in \mathcal{L}\mathcal{F}(x)$. Hence, in the sequel of the proof, we only consider the set of robot locations satisfying $x^* \notin \mathcal{L}\mathcal{F}(x)$.

Let $x \in \mathcal{F}$ such that $x^* \notin \mathcal{L}\mathcal{F}(x)$. Recall from (7) and (9) that $\mathcal{L}\mathcal{W}(x)$ is determined by the maximum margin separating hyperplanes of the robot body and obstacles, and $\mathcal{L}\mathcal{F}(x)$ is obtained by eroding $\mathcal{L}\mathcal{W}(x)$ by an open ball of radius r . Hence, x lies in the interior of $\mathcal{L}\mathcal{F}(x)$ if and only if $d(x, O_i) > r$ for all i . As a result, since $x^* \notin \mathcal{L}\mathcal{F}(x)$, one has $x = \Pi_{\mathcal{L}\mathcal{F}(x)}(x^*)$ only if $d(x, O_i) = r$ for some i .

Note that if $d(x, O_i) = r$, then, since $d(O_i, O_j) > 2r$ (Assumption 1), $d(x, O_j) > r$ for all $j \neq i$. Therefore, there can be only one obstacle index i such that $x = \Pi_{\mathcal{L}\mathcal{W}(x)}(x^*)$ and $d(x, O_i) = r$. Further, given $d(x, O_i) = r$, since $\Pi_{\mathcal{L}\mathcal{F}(x)}(x^*)$ is the unique closest point of the closed convex set $\mathcal{L}\mathcal{F}(x)$ to the goal x^* (Theorem 2), its optimality [6] implies that one has $x = \Pi_{\mathcal{L}\mathcal{W}(x)}(x^*)$ if and only if the maximum margin separating hyperplane between the robot and obstacle O_i is tangent to the level curve of the squared Euclidean distance to the goal, $\|x - x^*\|^2$, at $\Pi_{\overline{O}_i}(x)$, and separates x and x^* , i.e.,

$$\frac{(x - \Pi_{\overline{O}_i}(x))^T (x - x^*)}{\|x - \Pi_{\overline{O}_i}(x)\| \|x - x^*\|} = 1. \quad (12)$$

Thus, one can locate the stationary points of the “move-to-projected-goal” law in (10) associated with obstacle O_i as in (11), and so the result follows. ■

Note that, for any equilibrium point $s_i \in \mathfrak{S}_i$ associated with obstacle O_i , one has that the equilibrium s_i , its projection $\Pi_{\overline{O}_i}(s_i)$ and the goal x^* are all collinear.

Lemma 2 *The “move-to-projected-goal” law (10) in a small neighborhood of the goal x^* is given by*

$$u(x) = -k(x - x^*), \quad \forall x \in B(x^*, \epsilon), \quad (13)$$

for some $\epsilon > 0$; and around any stationary point $s_i \in \mathfrak{S}_i$ (11), associated with obstacle O_i , it is given by

$$u(x) = -k \left(x - x^* + \frac{(x - \Pi_{\overline{O}_i}(x))^T (x^* - h_i)}{\|x - \Pi_{\overline{O}_i}(x)\|^2} (x - \Pi_{\overline{O}_i}(x)) \right), \quad (14)$$

for all $x \in B(s_i, \epsilon)$ and some $\epsilon > 0$, where

$$h_i := \frac{x + \Pi_{\overline{O}_i}(x)}{2} + \frac{r}{2} \frac{x - \Pi_{\overline{O}_i}(x)}{\|x - \Pi_{\overline{O}_i}(x)\|}. \quad (15)$$

Proof: See Appendix I-C.

Since our “move-to-projected-goal” law strictly decreases the (squared) Euclidean distance to the goal x^* away from its stationary points (Proposition 7), to guarantee the existence of a unique stable attractor at x^* we require the following assumption¹², whose geometric interpretation is discussed in detail in Appendix II.

Assumption 2 (*Obstacle Curvature Condition*) *The Jacobian matrix $\mathbf{J}_{\Pi_{\overline{O}_i}}(s_i)$ of the metric projection of any stationary point $s_i \in \mathfrak{S}_i$ onto the associated obstacle O_i satisfies¹³*

$$\mathbf{J}_{\Pi_{\overline{O}_i}}(s_i) \prec \frac{\|x^* - \Pi_{\overline{O}_i}(s_i)\|}{r + \|x^* - \Pi_{\overline{O}_i}(s_i)\|} \mathbf{I} \quad \forall i, \quad (16)$$

where \mathbf{I} is the identity matrix of appropriate size.

Proposition 6 *If Assumption 2 holds for the goal x^* and for all obstacles, then x^* is the only locally stable equilibrium of the “move-to-projected-goal” law (10), and all the stationary points, $s_i \in \mathfrak{S}_i$ (11), associated with obstacles, O_i , are nondegenerate saddles.*

Proof: It follows from (13) that the goal x^* is a locally stable point of the “move-to-projected-goal” law, because its Jacobian matrix, $\mathbf{J}_u(x^*)$, at x^* is equal to $-k\mathbf{I}$.

Now, to determine the type of any stationary point $s_i \in \mathfrak{S}_i$ associated with obstacle O_i , define

$$g(x) := \frac{(x^* - \Pi_{\overline{O}_i}(x))^T (x - \Pi_{\overline{O}_i}(x))}{\|x - \Pi_{\overline{O}_i}(x)\|^2} - \frac{r}{2\|x - \Pi_{\overline{O}_i}(x)\|} - \frac{1}{2}, \quad (17)$$

and so the “move-to-projected-goal” law in a small neighborhood of s_i in (14) can be rewritten as

$$\dot{u}(x) = -k \left(x - x^* + g(x)(x - \Pi_{\overline{O}_i}(x)) \right). \quad (18)$$

Hence, using $\|s_i - \Pi_{\overline{O}_i}(s_i)\| = r$, one can verify that its Jacobian matrix at s_i is given by

$$\mathbf{J}_u(s_i) = -kg(s_i) \left(\frac{\|x^* - \Pi_{\overline{O}_i}(s_i)\|}{r + \|x^* - \Pi_{\overline{O}_i}(s_i)\|} \mathbf{Q} - \mathbf{J}_{\Pi_{\overline{O}_i}}(s_i) \right) - \frac{k}{2} (\mathbf{I} - \mathbf{Q}), \quad (19)$$

where $g(s_i) = -\frac{\|x^* - \Pi_{\overline{O}_i}(s_i)\|}{r} - 1 < -2$, and

$$\mathbf{Q} = \mathbf{I} - \frac{(s_i - \Pi_{\overline{O}_i}(s_i))(s_i - \Pi_{\overline{O}_i}(s_i))^T}{\|s_i - \Pi_{\overline{O}_i}(s_i)\|^2}. \quad (20)$$

Note that $\mathbf{J}_{\Pi_{\overline{O}_i}}(x)(x - \Pi_{\overline{O}_i}(x)) = 0$ for all $x \in \mathbb{R}^n \setminus \overline{O}_i$ [19, 24]. Hence, if Assumption 2 holds, then one can conclude from $g(s_i) < -2$ and (19) that the only negative eigenvalue of $\mathbf{J}_u(s_i)$ and the associated eigenvector are $-\frac{k}{2}$ and $(s_i - \Pi_{\overline{O}_i}(s_i))$, respectively; and all other eigenvalues of $\mathbf{J}_u(s_i)$ are positive. Thus, s_i is a nondegenerate saddle point of the “move-to-projected-goal” law associated with O_i . ■

¹²A similar obstacle curvature condition is necessarily made in the design of navigation functions for spaces with convex obstacles in [42].

¹³For any two symmetric matrices $\mathbf{A}, \mathbf{B} \in \mathbb{R}^{N \times N}$, $\mathbf{A} \prec \mathbf{B}$ (and $\mathbf{A} \preceq \mathbf{B}$) means that $\mathbf{B} - \mathbf{A}$ is positive definite (positive semidefinite, respectively).

■ **Proposition 7** *Given that the goal location x^* and obstacles satisfy Assumption 2, the goal x^* is an asymptotically stable equilibrium of the “move-to-projected-goal” law (10), whose basin of attraction includes \mathcal{F} , except a set of measure zero.*

Proof: Consider the squared Euclidean distance to the goal as a smooth Lyapunov function candidate, i.e., $V(x) := \|x - x^*\|^2$, and it follows from (4) and (10) that

$$\dot{V}(x) = -k \underbrace{2(x - x^*)^T (x - \Pi_{\mathcal{L}\mathcal{F}(x)}(x^*))}_{\geq \|x - \Pi_{\mathcal{L}\mathcal{F}(x)}(x^*)\|^2}, \quad (21)$$

$$\begin{aligned} & \text{since } x \in \mathcal{L}\mathcal{F}(x) \text{ and } \|x - x^*\|^2 \geq \|\Pi_{\mathcal{L}\mathcal{F}(x)}(x^*) - x^*\|^2 \\ & \leq -k \|x - \Pi_{\mathcal{L}\mathcal{F}(x)}(x^*)\|^2 \leq 0, \end{aligned} \quad (22)$$

which is zero iff x is a stationary point. Hence, we have from LaSalle’s Invariance Principle [27] that all robot configurations in \mathcal{F} asymptotically reach the set of equilibria of (10). Therefore, the result follows from Proposition 2 and Proposition 6, because, under Assumption 2, x^* is the only stable stationary point of the piecewise continuous “move-to-projected-goal” law (10), and all other stationary points are nondegenerate saddles whose stable manifolds have empty interiors [23]. ■

Finally, we find it useful to summarize important qualitative properties of the “move-to-projected-goal” law as:

Theorem 3 *The piecewise continuously differentiable “move-to-projected-goal” law in (10) leaves the robot’s free space \mathcal{F} (1) positively invariant; and if Assumption 2 holds, then its unique continuously differentiable flow, starting at almost any configuration $x \in \mathcal{F}$, asymptotically reaches the goal location x^* , while strictly decreasing the squared Euclidean distance to the goal, $\|x - x^*\|^2$, along the way.*

C. Extensions for Limited Range Sensing Modalities

1) *Navigation using a Fixed Radius Sensory Footprint:* A crucial property of the “move-to-projected-goal” law (10) is that it only requires the knowledge of the robot’s Voronoi-adjacent¹⁰ obstacles to determine the robot’s local workspace and so the robot’s local free space. We now exploit that property to relax our construction so that it can be put to practical use with commonly available sensors that have bounded radius footprint.¹⁴ We will present two specific instances, pointing out along the way how they nevertheless preserve the sufficient conditions for the qualitative properties listed in Section IV-B.

Suppose the robot is equipped with a sensor with a fixed sensing range, $R \in \mathbb{R}_{>0}$, whose sensory output, denoted by $\mathcal{S}_R(x) := \{S_1, S_2, \dots, S_m\}$, at a location, $x \in \mathcal{W}$, returns some computationally effective dense representation of the perceptible portion, $S_i := O_i \cap B(x, R)$, of each obstacle, O_i , in its sensory footprint, $B(x, R)$. Note that S_i is always open and might possibly be empty (if O_i is outside the robot’s sensing range), see Fig. 2(middle); and we assume that the robot’s sensing range is greater than the robot body radius, i.e., $R > r$.

¹⁴ This extension results from the construction of the robot’s local workspace (7) in terms of the maximum margin separating hyperplanes of convex sets. In consequence, because the intersection of convex sets is a convex set [6], perceived obstacles in the robot’s (convex) sensory footprint are, in turn, themselves always convex.

As in (7), using the maximum margin separating hyperplanes of the robot and sensed obstacles, we define the robot's *sensed local workspace*, illustrated in Fig. 2(middle), as,

$$\mathcal{LW}_s(x) := \left\{ q \in \mathcal{W} \cap \overline{B(x, \frac{r+R}{2})} \mid \left\| q - x + r \frac{x - \Pi_{\overline{S}_i}(x)}{\|x - \Pi_{\overline{S}_i}(x)\|} \right\| \leq \|q - \Pi_{\overline{S}_i}(x)\|, \forall i \text{ s.t. } S_i \neq \emptyset \right\}. \quad (23)$$

Note that $\overline{B(x, \frac{r+R}{2})}$ is equal to the intersection of the closed half spaces containing the robot body and defined by the maximum margin separating hyperplanes of the robot body, $\overline{B(x, r)}$, and all individual points, $q \in \mathbb{R}^n \setminus B(x, R)$, outside its sensory footprint.

An important observation revealing a critical connection between the robot's local workspace \mathcal{LW} in (7) and its sensed local workspace \mathcal{LW}_s in (23) is:

Proposition 8 $\mathcal{LW}_s(x) = \mathcal{LW}(x) \cap \overline{B(x, \frac{r+R}{2})}$ for all $x \in \mathcal{W}$.

Proof: See Appendix I-D. ■

In accordance with its local free space $\mathcal{LF}(x)$ in (9), we define the robot's *sensed local free space* $\mathcal{LF}_s(x)$ by eroding $\mathcal{LW}_s(x)$ by the robot body, illustrated in Fig. 2(middle), as,

$$\mathcal{LF}_s(x) := \left\{ q \in \mathcal{LW}_s(x) \mid \overline{B(q, r)} \subseteq \mathcal{LW}_s(x) \right\}, \quad (24a)$$

$$= \mathcal{LF}(x) \cap \overline{B(x, \frac{R-r}{2})}, \quad (24b)$$

where the latter follows from Proposition 8 and that the erosion operation is distributed over set intersection [21]. Note that, for any $x \in \mathcal{F}$, $\mathcal{LF}_s(x)$ is a nonempty closed convex set containing x as is $\mathcal{LF}(x)$.

To safely steer a single-integrator disk-shaped robot towards a given goal location $x^* \in \mathcal{F}$ using a fixed radius sensory footprint, we propose the following “move-to-projected-goal” law,

$$u(x) = -k(x - \Pi_{\mathcal{LF}_s(x)}(x^*)), \quad (25)$$

where $k > 0$ is a fixed control gain, and $\Pi_{\mathcal{LF}_s(x)}$ (4) is the metric projection onto the robot's sensed local free space $\mathcal{LF}_s(x)$, and $\mathcal{LF}_s(x)$ is assumed to be continuously updated.

Due to the nice relations between the robot's different local neighborhoods in Proposition 8 and (24b), the revised “move-to-projected-goal” law for a fixed radius sensory footprint inherits all qualitative properties of the original one presented in Section IV-B, summarized as:

Proposition 9 *The “move-to-projected-goal” law of a disk-shaped robot equipped with a fixed radius sensory footprint in (25) is piecewise continuously differentiable; and if Assumption 2 holds, then its unique continuously differentiable flow asymptotically steers almost all configurations in its positively invariant domain \mathcal{F} towards any given goal location $x^* \in \mathcal{F}$, while strictly decreasing the (squared) Euclidean distance to the goal along the way.*

Proof: The proof of the result follows patterns similar to those of Proposition 2 - Proposition 7, because of the relations between the robot's local neighborhoods in Proposition 8 and (24b), and so it is omitted for the sake of brevity. ■

2) *Navigation using a 2D LIDAR Range Scanner:* We now present another practical extension of the “move-to-projected-goal” law for safe robot navigation using a 2D LIDAR range scanner in an unknown convex planar environment $\mathcal{W} \subseteq \mathbb{R}^2$ populated with convex obstacles $\mathcal{O} = \{O_1, O_2, \dots, O_m\}$, satisfying Assumption 1. Assuming an angular scanning range of 360 degrees and a fixed radial range of $R \in \mathbb{R}_{>0}$, we model the sensory measurement of the LIDAR scanner at location $x \in \mathcal{W}$ by a polar curve [48] $\rho_x : (-\pi, \pi) \rightarrow [0, R]$, defined as,

$$\rho_x(\theta) := \min \left(\begin{array}{c} R, \\ \min \left\{ \|p-x\| \mid p \in \partial\mathcal{W}, \text{atan2}(p-x) = \theta \right\}, \\ \min_i \left\{ \|p-x\| \mid p \in O_i, \text{atan2}(p-x) = \theta \right\} \end{array} \right). \quad (26)$$

We further assume that the LIDAR sensing range is greater than the robot body radius, i.e., $R > r$.

Suppose $\rho_i : (\theta_{l_i}, \theta_{u_i}) \rightarrow [0, R]$ is a convex curve segment of the LIDAR scan ρ_x (26) at location $x \in \mathcal{W}$ (please refer to Appendix V for the notion of convexity in polar coordinates which we use to identify convex polar curve segments in a LIDAR scan, corresponding to the obstacle and workspace boundary), then we define the associated *line-of-sight obstacle* as the open epigraph of ρ_i whose pole is located at x [48],^{8 15}

$$L_i := \{x\} \oplus \text{epi}\rho_i, \quad (27)$$

$$= \{x\} \oplus \left\{ (\varrho \cos \theta, \varrho \sin \theta) \mid \theta \in (\theta_{l_i}, \theta_{u_i}), \varrho > \rho_i(\theta) \right\}, \quad (28)$$

which is an open convex set. Accordingly, we assume the availability of a sensor model $\mathcal{L}_R(x) := \{L_1, L_2, \dots, L_t\}$ that returns the list of convex line-of-sight obstacles detected by the LIDAR scanner at location x , where t denotes the number of detected obstacles and changes as a function of robot location.

Following the lines of (7) and (9), we define the robot's *line-of-sight local workspace* and *line-of-sight local free space*, illustrated in Fig. 2(right), respectively, as

$$\mathcal{LW}_\mathcal{L}(x) := \left\{ q \in L_{ft}(x) \cap \overline{B(x, \frac{r+R}{2})} \mid \left\| q - x + r \frac{x - \Pi_{\overline{L}_i}(x)}{\|x - \Pi_{\overline{L}_i}(x)\|} \right\| \leq \|q - \Pi_{\overline{L}_i}(x)\|, \forall i \right\}. \quad (29)$$

$$\mathcal{LF}_\mathcal{L}(x) := \left\{ q \in \mathcal{LW}_\mathcal{L}(x) \mid \overline{B(q, r)} \subseteq \mathcal{LW}_\mathcal{L}(x) \right\}, \quad (30)$$

where $L_{ft}(x)$ denotes the LIDAR sensory footprint at x , given by the hypograph of the LIDAR scan ρ_x (26) at x , i.e.,

$$L_{ft}(x) := \{x\} \oplus \text{hyp}\rho_x, \quad (31)$$

$$= \{x\} \oplus \left\{ (\varrho \cos \theta, \varrho \sin \theta) \mid \theta \in (-\pi, \pi], 0 \leq \varrho \leq \rho_x(\theta) \right\}. \quad (32)$$

Similar to Proposition 1 and Corollary 1, we have:

Proposition 10 *For any $x \in \mathcal{F}$, $\mathcal{LW}_\mathcal{L}(x)$ is an obstacle free closed convex subset of \mathcal{W} and contains the robot body $B(x, r)$. Therefore, $\mathcal{LF}_\mathcal{L}(x)$ is a nonempty closed convex subset of \mathcal{F} and contains x .*

Proof: See Appendix I-E. ■

¹⁵Here, $\overset{\circ}{A}$ denotes the interior of a set A .

Accordingly, to navigate a fully-actuated single-integrator robot using a LIDAR scanner towards a desired goal location $x^* \in \mathcal{F}$, with the guarantee of no collisions along the way, we propose the following “move-to-projected-goal” law

$$u(x) = -k(x - \Pi_{\mathcal{L}\mathcal{F}_L(x)}(x^*)), \quad (33)$$

where $k > 0$ is fixed, and $\Pi_{\mathcal{L}\mathcal{F}_L(x)}$ (4) is the metric projection onto the robot’s line-of-sight free space $\mathcal{L}\mathcal{F}_L(x)$ (30), which is assumed to be continuously updated.

We summarize important properties of the “move-to-projected-goal” law for navigation using a LIDAR scanner as:

Proposition 11 *The “move-to-projected-goal” law of a LIDAR-equipped disk-shaped robot in (33) leaves the robot’s free space \mathcal{F} (1) positively invariant; and if Assumption 2 holds, then its unique, continuous and piecewise differentiable flow asymptotically brings all but a measure zero set of initial configurations in \mathcal{F} to any designated goal location $x^* \in \mathcal{F}$, while strictly decreasing the (squared) Euclidean distance to the goal along the way.*

Proof: See Appendix I-F. ■

As a final remark, it is useful to note that the “move-to-projected-goal” law in (33) might have discontinuities because of possible occlusions between obstacles. If there is no occlusion between obstacles in the LIDAR’s sensing range, then the LIDAR scanner provides exactly the same information about obstacles as does the fixed radius sensory footprint of Section IV-C1, and so the “move-to-projected-goal” law in (33) is piecewise continuously differentiable as is its version in (25). In this regard, one can avoid occlusions between obstacles by properly selecting the LIDAR’s sensing range: for example, since $d(x, O_i) \geq r$ for any $x \in \mathcal{F}$ and $d(O_i, O_j) > 2r$ for any $i \neq j$ (Assumption 1), a conservative choice of R that prevents occlusions between obstacles is $r < R \leq 3r$.

D. An Extension for Differential Drive Robots

Maintaining the specialization to the plane, $\mathcal{W} \subset \mathbb{R}^2$, we now consider a disk-shaped differential drive robot described by state $(x, \theta) \in \mathcal{F} \times (-\pi, \pi]$, centered at $x \in \mathcal{F}$ with body radius $r \in \mathbb{R}_{>0}$ and orientation $\theta \in (-\pi, \pi]$, moving in \mathcal{W} . The kinematic equations describing its motion are

$$\dot{x} = v \begin{bmatrix} \cos \theta \\ \sin \theta \end{bmatrix}, \quad \text{and} \quad \dot{\theta} = \omega, \quad (34)$$

where $v \in \mathbb{R}$ and $\omega \in \mathbb{R}$ are, respectively, the linear (tangential) and angular velocity inputs of the robot.

In contrary to the “move-to-projected-goal” law of a fully actuated robot in (10), a differential drive robot can not directly move towards the projected goal $\Pi_{\mathcal{L}\mathcal{F}(x)}(x^*)$ of a given goal location $x^* \in \mathring{\mathcal{F}}$, unless it is perfectly aligned with $\Pi_{\mathcal{L}\mathcal{F}(x)}(x^*)$, because it is underactuated due to the nonholonomic constraint $\begin{bmatrix} -\sin \theta \\ \cos \theta \end{bmatrix}^T \dot{x} = 0$.¹⁶ In consequence, to determine the robot’s linear motion, we restrict the robot’s local free space $\mathcal{L}\mathcal{F}(x)$ (9) to conform to the nonholonomic constraint as

$$\mathcal{L}\mathcal{F}_v(x) := \mathcal{L}\mathcal{F}(x) \cap H_N, \quad (35)$$

where $H_N := \left\{ q \in \mathbb{R}^n \mid \begin{bmatrix} -\sin \theta \\ \cos \theta \end{bmatrix}^T (q - x) = 0 \right\}$ is the straight line motion range due to the nonholonomic constraint. Note that $\mathcal{L}\mathcal{F}(x) \cap H_N$ is a closed line segment in \mathcal{W} and contains x . Similarly, to determine the robot’s angular motion, we define

$$\mathcal{L}\mathcal{F}_\omega(x) := \mathcal{L}\mathcal{F}(x) \cap H_G, \quad (36)$$

where $H_G := \{ \omega x + (1 - \omega)x^* \in \mathbb{R}^n \mid \omega \in \mathbb{R} \}$ is the line going through x and x^* .

Accordingly, based on a standard differential drive controller [3], we propose the following “move-to-projected-goal” law for a differential drive robot,^{17 18}

$$v = -k \begin{bmatrix} \cos \theta \\ \sin \theta \end{bmatrix}^T (x - \Pi_{\mathcal{L}\mathcal{F}_v(x)}(x^*)), \quad (37a)$$

$$\omega = k \operatorname{atan} \left(\frac{\begin{bmatrix} -\sin \theta \\ \cos \theta \end{bmatrix}^T \left(x - \frac{\Pi_{\mathcal{L}\mathcal{F}_\omega(x)}(x^*) + \Pi_{\mathcal{L}\mathcal{F}(x)}(x^*)}{2} \right)}{\begin{bmatrix} \cos \theta \\ \sin \theta \end{bmatrix}^T \left(x - \frac{\Pi_{\mathcal{L}\mathcal{F}_\omega(x)}(x^*) + \Pi_{\mathcal{L}\mathcal{F}(x)}(x^*)}{2} \right)} \right), \quad (37b)$$

where $k > 0$ is fixed, and $\mathcal{L}\mathcal{F}_v(x)$, $\mathcal{L}\mathcal{F}_\omega(x)$ and $\mathcal{L}\mathcal{F}(x)$ are assumed to be continuously updated.

We summarize some important properties of the “move-to-projected-goal” law of a differential drive robot as:

Proposition 12 *Given the goal and obstacles satisfy Assumption 2, the “move-to-projected-goal” law of a disk-shaped differential drive robot in (37) asymptotically steers almost all configurations in its positively invariant domain $\mathcal{F} \times (-\pi, \pi]$ towards any given goal location $x^* \in \mathring{\mathcal{F}}$, without increasing the Euclidean distance to the goal along the way.*

Proof: See Appendix I-G. ■

Note that the “move-to-projected-goal” law of a differential drive robot in (37) can be extended to limited range sensing models by using the robot’s sensed local free space $\mathcal{L}\mathcal{F}_S$ (24) or the robot’s line-of-sight local free space $\mathcal{L}\mathcal{F}_L$ (30) instead of the local free space $\mathcal{L}\mathcal{W}$ (9), and the resulting vector field planner maintains qualitative properties.

V. NUMERICAL SIMULATIONS

To demonstrate the motion pattern generated by our “move-to-projected-goal” law around and far away from the goal, we consider a 10×10 and a 50×10 environment cluttered with convex obstacles and a desired goal located at around the upper right corner, as illustrated in Fig. 3 and Fig. 4, respectively.¹⁹ We present in these figures example navigation trajectories of the “move-to-projected-goal” law for different sensing and actuation modalities. We observe a significant

¹⁶Here, we require the goal to be in the interior $\mathring{\mathcal{F}}$ of \mathcal{F} to guarantee that the robot can nearly align its orientation with the (local) goal in finite time.

¹⁷We follow [3] by resolving the indeterminacy through setting $\omega = 0$ whenever $x = \frac{\Pi_{\mathcal{L}\mathcal{F}_\omega(x)}(x^*) + \Pi_{\mathcal{L}\mathcal{F}(x)}(x^*)}{2}$. Note that this introduces the discontinuity necessitated by Brockett’s condition [7].

¹⁸In the design of angular motion we particularly select a local target location, $\frac{\Pi_{\mathcal{L}\mathcal{F}_\omega(x)}(x^*) + \Pi_{\mathcal{L}\mathcal{F}(x)}(x^*)}{2} \in \mathring{\mathcal{F}}$ given $x^* \in \mathring{\mathcal{F}}$, in the interior $\mathring{\mathcal{F}}$ of \mathcal{F} to increase the convergence rate of the resulting vector field. One can consider other convex combinations of $\Pi_{\mathcal{L}\mathcal{F}_\omega(x)}(x^*)$ and $\Pi_{\mathcal{L}\mathcal{F}(x)}(x^*)$, and the resulting vector field retains qualitative properties.

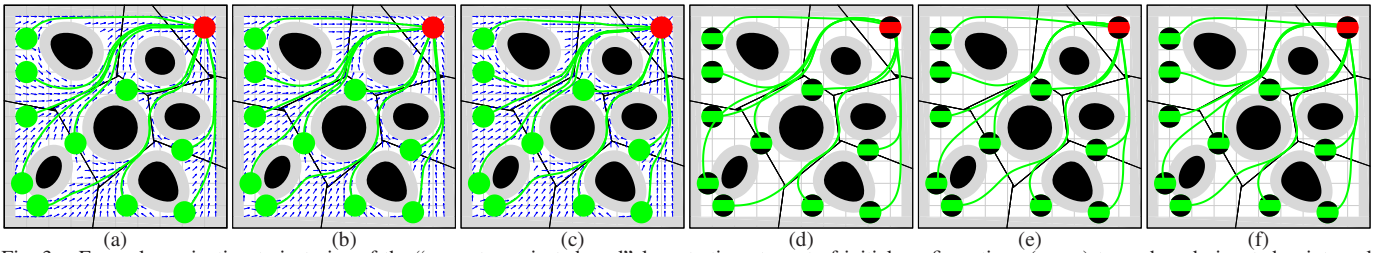


Fig. 3. Example navigation trajectories of the “move-to-projected-goal” law starting at a set of initial configurations (green) towards a designated point goal (red) for different sensing and actuation models: (a,b,c) a fully actuated robot, (d,e,f) a differential drive robot, (a,d) Voronoi-adjacent¹⁰ obstacle sensing, (b,e) a fixed radius sensory footprint, (c,f) a limited range LIDAR sensor.

consistency between the resulting trajectories of the “move-to-projected-goal” law and the boundary of the Voronoi diagram of the environment, where the robot balances its distance to all proximal obstacles while navigating towards its destination — a desired autonomous behaviour for many practical settings instead of following the obstacle boundary tightly. In our simulations, we avoid occlusions between obstacles by properly selecting the LIDAR’s sensing range, and in so doing both limited range sensing models provide the same information about the environment away from the workspace boundary and the associated “move-to-projected-goal” laws yield almost the same navigation paths. As observed in Fig. 3, although they are initiated at the same location, a fully actuated and a differential drive robot may follow significantly different trajectories due to their differences in system dynamics and controller design. It is also useful to note that the “move-to-projected-goal” law decreases not only the Euclidean distance, $\|x - x^*\|$, to the goal, but also the Euclidean distance, $\|\Pi_{\mathcal{L}\mathcal{F}(x)}(x^*) - x^*\|$, between the projected goal, $\Pi_{\mathcal{L}\mathcal{F}(x)}(x^*)$, and the global goal, x^* , illustrated in Fig. 5.



Fig. 5. The Euclidean distance, $\|\Pi_{\mathcal{L}\mathcal{F}(x)}(x^*) - x^*\|$, between the projected goal, $\Pi_{\mathcal{L}\mathcal{F}(x)}(x^*)$, and the global goal, x^* , for different sensing modalities: (left) Voronoi-adjacent¹⁰ obstacle sensing, (middle) a fixed radius sensory footprint, (right) a limited range line-of-sight sensor.

¹⁹For all simulations we set $r = 0.5$, $R = 2$ and $k = 1$, and all simulations are obtained through numerical integration of the associated “move-to-projected-goal” law using the `ode45` function of MATLAB.

VI. CONCLUSIONS

In this paper we construct a sensor-based feedback law that solves the real-time collision free robot navigation problem in a domain cluttered with convex obstacles. Our algorithm introduces a novel use of separating hyperplanes for identifying the robot’s local obstacle free convex neighborhood, affording a piecewise smooth velocity command instantaneously pointing toward the metric projection of the designated goal location onto this convex set. Given separated and appropriately “strongly” convex obstacles, we show that the resulting vector field has a smooth flow with a unique attractor at the goal location (along with the topologically inevitable saddles — at least one for each obstacle). Since all of its critical points are nondegenerate, our vector field asymptotically steers almost all configurations in the robot’s free space to the goal, with the guarantee of no collisions along the way. We also present its practical extensions for two limited range sensing models and the widely used differential drive model, while maintaining formal guarantees. We illustrate the effectiveness of the proposed navigation algorithm in numerical simulations.

Work now in progress targets a fully smoothed version of the move-to-projected-goal law (by recourse to logarithmic barrier functions [6]), permitting its lift to more complicated dynamical models such as force-controlled (second order) and more severely underactuated systems. This will enable its empirical demonstration for safe, high-speed navigation in a forest-like environments and in human crowds. We are also investigating the extension of these ideas for coordinated, decentralized feedback control of multirobot swarms. More generally, we seek to identify fundamental limits on navigable environments for a memoryless greedy robotic agent with a limited range sensing capability.

²⁰Please refer to Appendix VII and see the accompanying video submission for additional figures illustrating the navigation pattern far away from the goal for different sensing and actuation models.

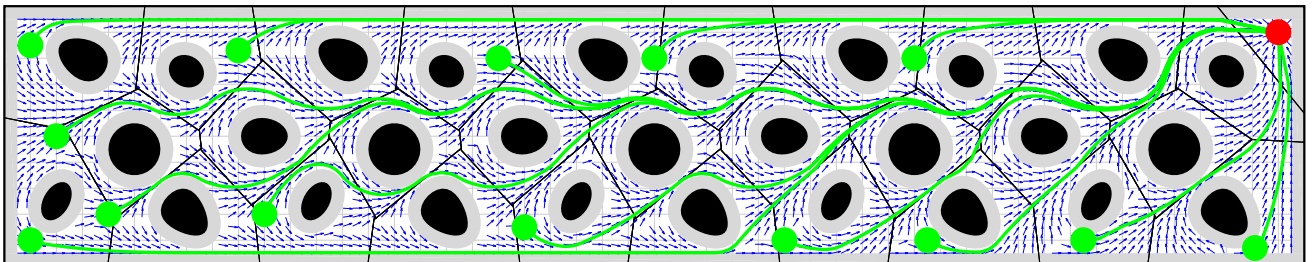


Fig. 4. Example navigation trajectories of the “move-to-projected-goal” law in (10) starting at a set of initial positions (green) far away from the goal (red).²⁰

APPENDIX I
PROOFS

A. Proof of Lemma 1

Proof: By definition (4), the metric projection $\Pi_{\bar{A}}(x)$ of the ball's centroid x onto the convex set \bar{A} is the unique closest point of \bar{A} to x . Hence, due to the symmetry of the ball, the closest point of $\overline{B(x, r)}$ to \bar{A} lies on the line segment joining x and $\Pi_{\bar{A}}(x)$, and is given by $(\Pi_{\overline{B(x, r)}} \circ \Pi_{\bar{A}})(x) = x - r \frac{x - \Pi_{\bar{A}}(x)}{\|x - \Pi_{\bar{A}}(x)\|}$, and so the closest point of \bar{A} to $\overline{B(x, r)}$ is $\Pi_{\bar{A}}(x)$. Thus, the result follows. ■

B. Proof of Proposition 1

Proof: To prove the result, it is convenient to rewrite (7) as $\mathcal{LW}(x) = \mathcal{W} \cap \bigcap_i HS_i$, where

$$HS_i := \left\{ q \in \mathbb{R}^n \mid \left\| q - x + r \frac{x - \Pi_{\overline{O_i}}(x)}{\|x - \Pi_{\overline{O_i}}(x)\|} \right\| \leq \|q - \Pi_{\overline{O_i}}(x)\| \right\}. \quad (38)$$

Note that for any $x \in \mathcal{F}$, HS_i is the half space defined by the maximum margin separating hyperplane between the robot body $\overline{B(x, r)}$ and obstacle O_i (Lemma 1), and contains the robot. Moreover, since O_i is open, we have $O_i \cap HS_i = \emptyset$ for any $x \in \mathcal{F}$.

Hence, using (1), one can verify the result as follows:

$$x \in \mathcal{F} \iff \begin{cases} \overline{B(x, r)} \subseteq \mathcal{W}, \\ \overline{B(x, r)} \cap O_i = \emptyset \quad \forall i, \end{cases} \quad (39)$$

$$\iff \begin{cases} \overline{B(x, r)} \subseteq \mathcal{W}, \\ \overline{B(x, r)} \subseteq HS_i \quad \forall i, \\ O_i \cap HS_i = \emptyset \quad \forall i, \end{cases} \quad (40)$$

$$\iff \begin{cases} \overline{B(x, r)} \subseteq \mathcal{LW}(x), \\ O_i \cap \mathcal{LW}(x) = \emptyset \quad \forall i, \end{cases} \quad (41)$$

which completes the proof. ■

C. Proof of Lemma 2

Proof: The result for the goal location x^* follows from the continuity of Voronoi diagrams in (6) and $x^* \in \mathcal{LF}(x^*)$.

To see the result for any stationary point $s_i \in \mathfrak{S}_i$, recall from the proof of Proposition 5 that s_i lies on the boundary segment of $\mathcal{LF}(s_i)$ defined by the separating hyperplane between the robot and i th obstacle, and s_i has a certain nonzero clearance from the boundary segment of $\mathcal{LF}(s_i)$ defined by the separating hyperplane between the robot and any other obstacle. Hence, using the continuity of Voronoi diagrams, for any $x \in B(s_i, \varepsilon)$ the ‘‘projected-goal’’ $\Pi_{\mathcal{LF}(x)}(x^*)$ can be located by taking the projection of x^* onto (a shifted version of) the maximum margin separating hyperplane between the robot and i th obstacle as

$$\Pi_{\mathcal{LF}(x)}(x^*) = x^* - \frac{(x - \Pi_{\overline{O_i}}(x))^T (x^* - h_i)}{\|x - \Pi_{\overline{O_i}}(x)\|^2} (x - \Pi_{\overline{O_i}}(x)), \quad (42)$$

where h_i is defined as in (15), and so this completes the proof. ■

D. Proof of Proposition 8

Proof: As discussed in the proof of Proposition 1, for any $x \in \mathcal{W}$ we have $\mathcal{LW}(x) = \mathcal{W} \cap \bigcap_i HS_i$, where HS_i is defined as in (38). Similarly, one can rewrite (23) as $\mathcal{LW}_g(x) = \mathcal{W} \cap \overline{B(x, \frac{r+R}{2})} \cap \bigcap_i \widehat{HS}_i$, where

$$\widehat{HS}_i := \left\{ q \in \mathbb{R}^n \mid \left\| q - x + r \frac{x - \Pi_{\overline{S_i}}(x)}{\|x - \Pi_{\overline{S_i}}(x)\|} \right\| \leq \|q - \Pi_{\overline{S_i}}(x)\| \right\}. \quad (43)$$

Note that if $S_i = \emptyset$, then the predicate in (43) is trivially holds and so $\widehat{HS}_i = \mathbb{R}^n$; otherwise, since $S_i = O_i \cap B(x, R)$, we have $\Pi_{\overline{S_i}}(x) = \Pi_{\overline{O_i}}(x)$ and so $\widehat{HS}_i = HS_i$. Moreover, if $S_i = \emptyset$ (i.e., $d(x, O_i) > R$), then we also have from Definition 1 and Lemma 1 that $\overline{B(x, \frac{r+R}{2})} \subset HS_i$. Thus, we obtain that

$$\widehat{HS}_i \cap \overline{B(x, \frac{r+R}{2})} = HS_i \cap \overline{B(x, \frac{r+R}{2})}, \quad \forall i. \quad (44)$$

Therefore, one can verify the result as follows:

$$\mathcal{LW}_g(x) = \mathcal{W} \cap \overline{B(x, \frac{r+R}{2})} \cap \bigcap_i \widehat{HS}_i, \quad (45)$$

$$= \mathcal{W} \cap \bigcap_i \left(\widehat{HS}_i \cap \overline{B(x, \frac{r+R}{2})} \right), \quad (46)$$

$$= \mathcal{W} \cap \bigcap_i \left(HS_i \cap \overline{B(x, \frac{r+R}{2})} \right), \quad (47)$$

$$= \left(\mathcal{W} \cap \bigcap_i HS_i \right) \cap \overline{B(x, \frac{r+R}{2})}, \quad (48)$$

$$= \mathcal{LW}(x) \cap \overline{B(x, \frac{r+R}{2})}. \quad (49)$$

■

E. Proof of Proposition 10

Proof: For any $x \in \mathcal{F}$ the LIDAR sensory footprint in (31) can be equivalently rewritten using the global knowledge of the robot's workspace as

$$L_{ft}(x) = \mathcal{W} \cap \overline{B(x, R)} \setminus \bigcup_i A_i. \quad (50)$$

where A_i is the augmented line-of-sight obstacle associated with obstacle O_i , defined as

$$A_i := \left\{ \alpha(p - x) + p \mid p \in O_i, \alpha \in [0, \infty) \right\}. \quad (51)$$

Hence, since $R > r$, it follows from (29) that

$$\mathcal{LW}_L(x) = \widehat{\mathcal{LW}}_L(x) \setminus \bigcup_i A_i, \quad (52)$$

where

$$\widehat{\mathcal{LW}}_L(x) := \left\{ q \in \mathcal{W} \cap \overline{B(x, \frac{r+R}{2})} \mid \left\| q - x + r \frac{x - \Pi_{\overline{L_i}}(x)}{\|x - \Pi_{\overline{L_i}}(x)\|} \right\| \leq \|q - \Pi_{\overline{L_i}}(x)\|, \forall i \right\}. \quad (53)$$

Note that, as discussed in the proof of Proposition 1, since $x \in \mathcal{F}$, $\widehat{\mathcal{LW}}_L(x)$ is a closed convex set and free of any line-of-sight obstacle L_i , i.e., $\widehat{\mathcal{LW}}_L(x) \cap L_i = \emptyset$ for all i ; and it contains the robot body, i.e., $\overline{B(x, r)} \subseteq \widehat{\mathcal{LW}}_L(x)$.

Now observe that if obstacle O_i is in the LIDAR's sensing range, i.e., $O_i \cap B(x, R) \neq \emptyset$, then $A_i \cap B(x, R) = L_j \cap B(x, R)$ for some j . Hence, since $\widehat{\mathcal{LW}}_{\mathcal{L}}(x)$ is free of line-of-sight obstacles, we have from (52) that $\mathcal{LW}_{\mathcal{L}}(x) = \widehat{\mathcal{LW}}_{\mathcal{L}}(x)$. Thus, the result follows since $\mathcal{LF}_{\mathcal{L}}(x)$ is the erosion of $\mathcal{LW}_{\mathcal{L}}(x)$ by the robot body radius r . ■

F. Proof of Proposition 11

Proof: As discussed in the proof of Proposition 3, the positive invariance of \mathcal{F} under the “move-to-projected-goal” law in (33) follows from that for any $x \in \mathcal{F}$ the robot's line-of-sight local free space $\mathcal{LF}_{\mathcal{L}}(x)$ (30) is an obstacle free closed convex subset of \mathcal{F} , and contains both x and $\Pi_{\mathcal{LW}_{\mathcal{L}}(x)}(x^*)$ (Proposition 10 and Theorem 2). Hence, $-k(x - \Pi_{\mathcal{LW}_{\mathcal{L}}(x)}(x^*)) \in T_x\mathcal{F}$ is either interior directed or, at worst, tangent to the boundary of \mathcal{F} .

The existence, uniqueness and continuity of its flow can be observed using a partitioning of \mathcal{F} such that the “move-to-projected-goal” law is piecewise continuously differentiable in each connected component of any partition element. Let D_t denote the set of collision free robot locations at which the number of detected line-of-sight obstacles is equal to $t \in \mathbb{N}$, i.e.,

$$D_t := \{x \in \mathcal{F} \mid |\mathcal{L}_R(x)| = t\}. \quad (54)$$

Recall that $\mathcal{L}_R(x) = \{L_1, L_2, \dots, L_t\}$ is our sensor model that returns the list of convex line-of-sight obstacles detected by the LIDAR at location x . Hence, the collection of D_t 's defines a partition of \mathcal{F} .

Now observe that D_t is generally disconnected and the “move-to-projected-goal” law is piecewise continuously differentiable when its domain is restricted to any connected component of D_t since each line-of-sight obstacle is associated with an open convex segment of a LIDAR scan and each connected component of D_t is uniquely associated with a certain collection of obstacles and workspace boundary segments. Hence, since a piecewise continuously differentiable function is Lipschitz continuous on a compact set [10, 27], the “move-to-projected-goal” law has a unique continuously differentiable flow in every connected component of D_t . Further, when the robot enters a connected component of D_t , it stays in that connected component for a nonzero time since a line-of-sight obstacle L_i is an open set and can not instantaneously appear or disappear under any continuous motion. Thus, the unique, continuous and piecewise differentiable flow of the move-to-projected-goal” law in \mathcal{F} is constructed by piecing together its unique, continuously differentiable trajectories in every connected component of D_t 's.

Finally, using a similar pattern to the proofs of Proposition 5 and Proposition 6, one can verify that the set of stationary points of (33) is $\{x^*\} \cup \bigcup_{i=1}^m \mathfrak{S}_i$, where \mathfrak{S}_i is defined as in (11); and if Assumption 2 holds, then the goal x^* is the only locally stable point of (33), and all the stationary points, \mathfrak{S}_i , associated with obstacles, O_i , are nondegenerate saddles. Moreover, as discussed in the proof of Proposition

7, the “move-to-projected-goal” law in (33) strictly decreases the (squared) Euclidean distance to x^* away from its stationary points, and so x^* is the unique attractor of (33) whose basin of attraction includes all but a measure zero set of \mathcal{F} . ■

G. Proof of Proposition 12

Proof: The positive invariance of $\mathcal{F} \times (-\pi, \pi]$ under the “move-to-projected-goal” law (37) and the existence and uniqueness of its flow can be established using similar patterns of the proofs of Proposition 2, Proposition 3 and Proposition 4, and the flow properties of the differential drive controller in [3].

As in the proof of Proposition 7, using the squared distance to goal, $V(x) = \|x - x^*\|^2$, as a smooth Lypunov function, one can verify the stability properties from (4), (34), and (37) as follows: for any $(x, \theta) \in \mathcal{F} \times (-\pi, \pi]$

$$\begin{aligned} \dot{V}(x) &= -k \underbrace{2(x - x^*)^T (x - \Pi_{\mathcal{LF}_v(x)}(x^*))}_{\geq \|x - \Pi_{\mathcal{LF}_v(x)}(x^*)\|^2}, \quad (55) \\ &\quad \text{since } x \in \mathcal{LF}_v(x) \text{ and } \|x - x^*\|^2 \geq \|\Pi_{\mathcal{LF}_v(x)}(x^*) - x^*\|^2 \\ &\leq -k \|x - \Pi_{\mathcal{LF}_v(x)}(x^*)\|^2 \leq 0. \quad (56) \end{aligned}$$

Hence, it follows from LaSalle Invariance Principle [27] that all configurations in $\mathcal{F} \times (-\pi, \pi]$ asymptotically reach the set of configurations where robots are located at the associated projected goal $\Pi_{\mathcal{LF}_v(x)}(x^*)$ at any arbitrary orientation,

$$\left\{ (x, \theta) \in \mathcal{F} \times (-\pi, \pi] \mid x = \Pi_{\mathcal{LF}_v(x)}(x^*) \right\}. \quad (57)$$

Note that for any fixed $\Pi_{\mathcal{LF}_v(x)}(x^*)$, $\Pi_{\mathcal{LF}_\omega(x)}(x^*)$ and $\Pi_{\mathcal{LF}(x)}(x^*)$ the standard differential drive controller asymptotically aligns the robot with $\frac{\Pi_{\mathcal{LF}_\omega(x)}(x^*) + \Pi_{\mathcal{LF}(x)}(x^*)}{2}$, i.e., $\begin{bmatrix} -\sin \theta \\ \cos \theta \end{bmatrix}^T \left(x - \frac{\Pi_{\mathcal{LF}_\omega(x)}(x^*) + \Pi_{\mathcal{LF}(x)}(x^*)}{2} \right) = 0$. Hence, using the optimality of metric projection in (4) one can conclude that $\Pi_{\mathcal{LF}_v(x)}(x^*) = \Pi_{\mathcal{LF}_\omega(x)}(x^*) = \Pi_{\mathcal{LF}(x)}(x^*)$ whenever $x = \Pi_{\mathcal{LF}_v(x)}(x^*)$ and $\begin{bmatrix} -\sin \theta \\ \cos \theta \end{bmatrix}^T \left(x - \frac{\Pi_{\mathcal{LF}_\omega(x)}(x^*) + \Pi_{\mathcal{LF}(x)}(x^*)}{2} \right) = 0$.

Therefore, using a similar approach as the proofs of Proposition 5, Lemma 2 and Proposition 6, one can verify that the set of stationary points of (37) is given by

$$\{x^*\} \times (-\pi, \pi] \cup \left\{ (s_i, \theta) \in \mathcal{F} \times (-\pi, \pi] \mid s_i \in \mathfrak{S}_i, \begin{bmatrix} -\sin \theta \\ \cos \theta \end{bmatrix}^T (s_i - x^*) = 0 \right\}, \quad (58)$$

where \mathfrak{S}_i is defined as in (11); and every robot configuration located at x^* is locally stable and all stationary points associated with obstacles are nondegenerate saddles with stable manifolds of measure zero. Thus, the result follows. ■

APPENDIX II

GEOMETRIC INTERPRETATION OF THE CURVATURE CONDITION

A convenient way of characterizing metric limitations, such as the obstacle curvature condition in Assumption 2, of the “move-to-projected-goal” law is in terms of the enclosing balls of the goal x^* , defined as:

Definition 2 The enclosing ball, $B_x := B(x^*, \|x - x^*\| - r)$, of the goal x^* associated with a robot location $x \in \mathbb{R}^n \setminus B(x^*, r)$

is the largest open ball, centered at x^* , that does not intersect with the robot body $B(x, r)$.

In other words, the enclosing ball B_x is the largest ball centered at the goal x^* such that a disk-shaped robot of radius r starting at location x can go around it without increasing the Euclidean distance to the goal.

Observe that for any stationary point $s_i \in \mathfrak{S}_i$ (11) associated with obstacle O_i , one has $B_{s_i} = B(x^*, \|x^* - \Pi_{\overline{O}_i}(s_i)\|)$ and $\Pi_{\overline{B}_{s_i}}(s_i) = \Pi_{\overline{O}_i}(s_i)$, because s_i , $\Pi_{\overline{O}_i}(s_i)$ and x^* are all collinear (Proposition 5). That is to say, B_{s_i} is tangent to (i.e. the osculating ball of) O_i at $\Pi_{\overline{O}_i}(s_i)$. Hence, we have

$$\Pi_{\overline{B}_{s_i}}(x) = \|x^* - \Pi_{\overline{O}_i}(s_i)\| \frac{x - x^*}{\|x - x^*\|} \quad \forall x \in \mathbb{R}^n \setminus \overline{B}_{s_i}, \quad (59)$$

and so the Jacobian matrix $\mathbf{J}_{\Pi_{\overline{B}_{s_i}}}(s_i)$ of the metric projection of s_i onto the associated enclosing ball B_{s_i} is given by

$$\mathbf{J}_{\Pi_{\overline{B}_{s_i}}}(s_i) = \frac{\|x^* - \Pi_{\overline{O}_i}(s_i)\|}{r + \|x^* - \Pi_{\overline{O}_i}(s_i)\|} \mathbf{Q}_i(s_i), \quad (60)$$

where

$$\mathbf{Q}_i(x) := \mathbf{I} - \frac{(x - \Pi_{\overline{O}_i}(x))(x - \Pi_{\overline{O}_i}(x))^T}{\|x - \Pi_{\overline{O}_i}(x)\|^2}, \quad \forall x \in \mathbb{R}^n \setminus \overline{O}_i. \quad (61)$$

Therefore, since $\mathbf{Q}_i(s_i) \preceq \mathbf{I}$, one can conclude that the upper bound in (16) of Assumption 2 is due to the enclosing ball B_{s_i} of the goal x^* associated with s_i . Because any path starting at $x \in \mathbb{R}^n$ along which the distance to the goal x^* is strictly decreasing should stay in B_x for all future time; and the ‘‘move-to-projected-goal’’ law yields such navigation paths (Theorem 3).

More precisely, the geometric connection between enclosing balls of the goal and the curvature condition in Assumption 2 can be established as follows:

Proposition 13 *Let $s_i \in \mathfrak{S}_i$ (11) be a critical point associated with obstacle O_i . If $\overline{O}_i \setminus \Pi_{\overline{O}_i}(s_i) \subset B_{s_i}$, then*

$$\mathbf{J}_{\Pi_{\overline{O}_i}}(s_i) \prec \frac{\|x^* - \Pi_{\overline{O}_i}(s_i)\|}{\|x^* - \Pi_{\overline{O}_i}(s_i)\| + r} \mathbf{I}. \quad (62)$$

Therefore, if $\overline{O}_i \setminus \Pi_{\overline{O}_i}(s_i) \subset B_{s_i}$ for all $i \in \{1, 2, \dots, m\}$ and $s_i \in \mathfrak{S}_i$, then Assumption 2 holds.

Proof: Since $\Pi_{\overline{B}_{s_i}}(s_i) = \Pi_{\overline{O}_i}(s_i)$, the result can be verified using a similar pattern of the proof of Lemma 8; here the only difference is that the entire \overline{O}_i , except $\Pi_{\overline{O}_i}(s_i)$, is strictly contained in B_{s_i} . ■

Alternatively, using functional representations of obstacles, one can verify Assumption 2 as follows:

Proposition 14 *Let each obstacle O_i be associated with a convex function $f_i : \mathbb{R}^n \rightarrow \mathbb{R}$ such that $O_i = f_i^{-1}(-\infty, c_i)$ for some $c_i \in \mathbb{R}$. Then, Assumption 2 holds if*

$$\frac{\nabla^2 f_i(\Pi_{\overline{O}_i}(s_i))}{\|\nabla f_i(\Pi_{\overline{O}_i}(s_i))\|} \succ \frac{1}{\|x^* - \Pi_{\overline{O}_i}(s_i)\|}, \quad (63)$$

for all $i \in \{1, 2, \dots, m\}$ and $s_i \in \mathfrak{S}_i$ (11).

Proof: Consider the enclosing ball B_{s_i} of the goal x^* associated with $s_i \in \mathfrak{S}_i$. We have from Definition 2 that $B_{s_i} = \beta^{-1}(-\infty, \|x^* - \Pi_{\overline{O}_i}(s_i)\|)$, where $\beta(x) := \|x - x^*\|^2$. Hence, it follows that

$$\frac{\nabla^2 \beta(\Pi_{\overline{B}_{s_i}}(s_i))}{\|\nabla \beta(\Pi_{\overline{B}_{s_i}}(s_i))\|} = \frac{1}{\|x^* - \Pi_{\overline{O}_i}(s_i)\|}. \quad (64)$$

Thus, since $\Pi_{\overline{B}_{s_i}}(s_i) = \Pi_{\overline{O}_i}(s_i)$, one can conclude the result from Lemma 6 and Lemma 7. ■

Two immediate corollaries of Proposition 13 and Proposition 14 for the case of spherical and ellipsoidal obstacles are:

Corollary 2 *If all obstacles are open balls, then Assumption 2 holds for any goal $x^* \in \mathcal{F}$.*

Corollary 3 *Let each obstacle O_i be an open ellipsoid defined as $O_i = f_i^{-1}(-\infty, c_i)$ for some $c_i \in \mathbb{R}$, where $f_i := (x - p_i)^T \mathbf{A}_i (x - p_i)$ and $\mathbf{A}_i \in \mathbb{R}^{n \times n}$ is symmetric positive definite. Then, Assumption 2 holds if*

$$\frac{\lambda_{\min}(\mathbf{A}_i)}{\lambda_{\max}(\mathbf{A}_i)} > \frac{\|p_i - \Pi_{\overline{O}_i}(s_i)\|}{\|x^* - \Pi_{\overline{O}_i}(s_i)\|}, \quad (65)$$

for all $i \in \{1, 2, \dots, m\}$ and $s_i \in \mathfrak{S}_i$, where $\lambda_{\min}(\mathbf{A}_i)$ and $\lambda_{\max}(\mathbf{A}_i)$ are, respectively, the minimum and maximum eigenvalues of \mathbf{A}_i .

Proof: The results follows from Proposition 14 and

$$\frac{\nabla^2 f_i(\Pi_{\overline{O}_i}(s_i))}{\|\nabla f_i(\Pi_{\overline{O}_i}(s_i))\|} = \frac{\mathbf{A}}{\|\mathbf{A}(p_i - \Pi_{\overline{O}_i}(s_i))\|}, \quad (66)$$

$$\succ \frac{\lambda_{\min}(\mathbf{A}_i)}{\lambda_{\max}(\mathbf{A}_i)} \frac{1}{\|p_i - \Pi_{\overline{O}_i}(s_i)\|} \mathbf{I}. \quad (67)$$

In consequence, one can briefly conclude that it is easier for a robot to navigate around obstacles more spherical (i.e., not too flat) and towards goal locations away from obstacles, while strictly decreasing the Euclidean distance to the goal.

APPENDIX III

UNIQUENESS OF MAXIMUM MARGIN SEPARATING HYPERPLANES

For any two disjoint convex sets $A, B \in \mathbb{R}^n$, there can be more than one pair of points $a \in \overline{A}$ and $b \in \overline{B}$ achieving $\|a - b\| = d(A, B)$; however, they all have the same maximum margin separating hyperplane:

Lemma 3 *Let $A, B \subset \mathbb{R}^n$ be two disjoint convex sets, and $a_1, a_2 \in A$ and $b_1, b_2 \in B$ be points with $\|a_1 - b_1\| = \|a_2 - b_2\| = d(A, B)$. Then, for any $x \in \mathbb{R}^n$, the following equality always holds*

$$(a_1 - b_1)^T \left(x - \frac{a_1 + b_1}{2} \right) = (a_2 - b_2)^T \left(x - \frac{a_2 + b_2}{2} \right). \quad (68)$$

Proof: First, to see that $a_1 - b_1 = a_2 - a_2$, consider

$$(a_1 - b_1)^T(a_2 - b_2) = (a_1 - b_1)^T \left(a_2 - \frac{a_1 + b_1}{2} \right) + (b_1 - a_1)^T \left(b_2 - \frac{a_1 + b_1}{2} \right), \quad (69)$$

$$= d(A, B)^2 + \frac{1}{2} \underbrace{(a_1 - b_1)^T(a_2 - a_1)}_{\geq 0, \text{ by Theorem 2}} + \frac{1}{2} \underbrace{(b_1 - a_1)^T(b_2 - b_1)}_{\geq 0, \text{ by Theorem 2}}, \quad (70)$$

$$\geq d(A, B)^2. \quad (71)$$

where the inequality follows from Theorem 2 since $\|a_1 - b_1\| = d(A, B) = d(a_1, B) = d(A, b_1)$. Moreover, it follows from the Cauchy-Schwartz inequality that

$$(a_1 - b_1)^T(a_2 - b_2) \leq \|a_1 - b_1\| \|a_2 - b_2\| = d(A, B)^2. \quad (72)$$

Hence, since $(a_1 - b_1)^T(a_2 - b_2) = \|a_1 - b_1\|^2 = \|a_2 - b_2\|^2$, one always has

$$a_1 - b_1 = a_2 - b_2. \quad (73)$$

Also observe from (70) that

$$(a_1 - b_1)^T(a_1 - a_2) = 0, \quad (74a)$$

$$(a_1 - b_1)^T(b_1 - b_2) = 0. \quad (74b)$$

Therefore, the result can be verified as follows:

$$(a_2 - b_2)^T \left(x - \frac{a_2 + b_2}{2} \right) = (a_1 - b_1)^T \left(x - \frac{a_2 + b_2}{2} \right), \quad (75)$$

$$= (a_1 - b_1)^T \left(x - \frac{a_1 + b_1}{2} \right) + \underbrace{(a_1 - b_1)^T \left(\frac{a_1 + b_1}{2} - \frac{a_2 + b_2}{2} \right)}_{=0, \text{ by (74)}}, \quad (76)$$

$$= (a_1 - b_1)^T \left(x - \frac{a_1 + b_1}{2} \right). \quad (77)$$

APPENDIX IV

ON THE JACOBIAN OF METRIC PROJECTION

A well known property of metric projections is being nonexpansive:

Lemma 4 ([51]) *The metric projection onto a closed convex set $A \subseteq \mathbb{R}^n$ is Lipschitz continuous with Lipschitz constant 1, i.e. $\|\Pi_A(x) - \Pi_A(y)\| \leq \|x - y\|$ for all $x, y \in \mathbb{R}^n$.*

Note that a Lipschitz function in \mathbb{R}^n is differentiable almost everywhere, and Π_A is piecewise continuously differentiable [32].

Lemma 5 [19, 24]) *The Jacobian $\mathbf{J}_{\Pi_K}(x)$ of the metric projection onto a closed convex set $K \subseteq \mathbb{R}^n$ with twice continuously differentiable (\mathcal{C}^2) boundary is a positive semi-definite and symmetric operator of norm at most unity, i.e.,*

$$0 \preceq \mathbf{J}_{\Pi_K}(x) \preceq \mathbf{I}, \quad \forall x \in \mathbb{R}^n \setminus K, \quad (78)$$

and one has $\mathbf{J}_{\Pi_K}(x)(x - \Pi_K(x)) = 0$.

The Jacobian matrix of the metric projection onto a convex set can be analytically obtained using its functional representation in terms of a level set of a convex function:

Lemma 6 *Let $K \in \mathbb{R}^n$ be a closed convex set associated with a twice continuously differentiable (\mathcal{C}^2) convex function $f : \mathbb{R}^n \rightarrow \mathbb{R}$ such that $K = f^{-1}(-\infty, c]$ for some $c \in \mathbb{R}$.*

Then, the Jacobian $\mathbf{J}_{\Pi_K}(x)$ of the metric projection of $x \in \mathbb{R}^n \setminus K$ onto K is given by ²¹

$$\mathbf{J}_{\Pi_K}(x) = \mathbf{Q}(\mathbf{I} + \mathbf{Q}\mathbf{P}\mathbf{Q})^{-1}\mathbf{Q} = \mathbf{Q} - \mathbf{I} + (\mathbf{I} + \mathbf{Q}\mathbf{P}\mathbf{Q})^{-1}, \quad (79)$$

where

$$\mathbf{Q} := \mathbf{I} - \frac{(x - \Pi_K(x))(x - \Pi_K(x))^T}{\|x - \Pi_K(x)\|^2}, \quad (80)$$

$$\mathbf{P} := \frac{\|x - \Pi_K(x)\|}{\|\nabla f(\Pi_K(x))\|} \nabla^2 f(\Pi_K(x)). \quad (81)$$

Proof: Using the relation between K and f , one can rewrite the metric project onto K as

$$\Pi_K(x) = \arg \min_{y \in K} \|y - x\| = \arg \min_{f(y) \leq c} \|y - x\|. \quad (82)$$

Further, due to the optimality of $\Pi_K(x)$, the outward surface normal of K at $\Pi_K(x)$ is given by $\frac{x - \Pi_K(x)}{\|x - \Pi_K(x)\|} = \frac{\nabla f(\Pi_K(x))}{\|\nabla f(\Pi_K(x))\|}$, and we have

$$x = \Pi_K(x) + \|x - \Pi_K(x)\| \frac{\nabla f(\Pi_K(x))}{\|\nabla f(\Pi_K(x))\|}. \quad (83)$$

Hence, using $\mathbf{J}_{\Pi_K}(x)(x - \Pi_K(x)) = 0$ (Lemma 5), the derivative of (83) yields

$$\mathbf{J}_{\Pi_K}(x) = (\mathbf{I} - \mathbf{Q}\mathbf{P})^{-1}\mathbf{Q}. \quad (84)$$

Note that it is not straightforward to observe that the closed form of $\mathbf{J}_{\Pi_K}(x)$ in (84) is positive definite and symmetric (Lemma 5). Alternatively, using the matrix identity $(\mathbf{I} + \mathbf{A}\mathbf{B})^{-1}\mathbf{A} = \mathbf{A}(\mathbf{I} + \mathbf{B}\mathbf{A})^{-1}$ [43] and $\mathbf{Q}\mathbf{Q} = \mathbf{Q}$, a more informative closed form of $\mathbf{J}_{\Pi_K}(x)$ can be obtained as follows:

$$\mathbf{J}_{\Pi_K}(x) = (\mathbf{I} - \mathbf{Q}\mathbf{P})^{-1}\mathbf{Q} = \underbrace{(\mathbf{I} - \mathbf{Q}\mathbf{Q}\mathbf{P})^{-1}\mathbf{Q}\mathbf{Q}}_{=\mathbf{Q}(\mathbf{I} - \mathbf{Q}\mathbf{P}\mathbf{Q})^{-1}}, \quad (85)$$

$$= \mathbf{Q}(\mathbf{I} - \mathbf{Q}\mathbf{P}\mathbf{Q})^{-1}\mathbf{Q}. \quad (86)$$

Alternatively, using a special case of Woodbury matrix identity (a.k.a. the matrix inversion lemma) [43],

$$(\mathbf{I} + \mathbf{Q}\mathbf{P})^{-1} = \mathbf{I} - \mathbf{Q}(\mathbf{I} + \mathbf{P}\mathbf{Q})^{-1}\mathbf{P}, \quad (87)$$

we also have

$$\mathbf{J}_{\Pi_K}(x) = (\mathbf{I} - \mathbf{Q}\mathbf{P})^{-1}\mathbf{Q} = (\mathbf{I} - \mathbf{Q}(\mathbf{I} + \mathbf{P}\mathbf{Q})^{-1}\mathbf{P})\mathbf{Q}, \quad (88)$$

$$= \mathbf{Q} - \mathbf{I} + \underbrace{\mathbf{I} - \mathbf{Q}(\mathbf{I} + \mathbf{P}\mathbf{Q}\mathbf{Q})^{-1}\mathbf{P}\mathbf{Q}}_{=(\mathbf{I} + \mathbf{Q}\mathbf{P}\mathbf{Q})^{-1}}, \quad (89)$$

$$= \mathbf{Q} - \mathbf{I} + (\mathbf{I} + \mathbf{Q}\mathbf{P}\mathbf{Q})^{-1}. \quad (90)$$

Recall that $\mathbf{Q}\mathbf{Q} = \mathbf{Q}$. Thus, the lemma follows. \blacksquare

²¹Here, $\nabla f : \mathbb{R}^n \rightarrow \mathbb{R}^n$ and $\nabla^2 f : \mathbb{R}^n \rightarrow \mathbb{R}^{n \times n}$ denote the gradient and Hessian of a twice continuously differentiable function $f : \mathbb{R}^n \rightarrow \mathbb{R}$, respectively.

Lemma 7 Let $K_1, K_2 \in \mathbb{R}^n$ be two closed convex sets associated with twice differentiable convex functions $f_1 : \mathbb{R}^n \rightarrow \mathbb{R}$ and $f_2 : \mathbb{R}^n \rightarrow \mathbb{R}$, respectively, such that $K_1 = f_1^{-1}(-\infty, c_1]$ and $K_2 = f_2^{-1}(-\infty, c_2]$ for some $c_1, c_2 \in \mathbb{R}$. And let $x \in \mathbb{R}^n \setminus (K_1 \cup K_2)$ with $\Pi_{K_1}(x) = \Pi_{K_2}(x)$.

Then the following equivalence holds

$$\frac{\nabla^2 f_1(\Pi_{K_1}(x))}{\|\nabla f_1(\Pi_{K_1}(x))\|} \preceq \frac{\nabla^2 f_2(\Pi_{K_2}(x))}{\|\nabla f_2(\Pi_{K_2}(x))\|} \iff \mathbf{J}_{\Pi_{K_1}}(x) \succcurlyeq \mathbf{J}_{\Pi_{K_2}}(x). \quad (91)$$

Proof: The result directly follows from Lemma 6 and the following matrix relation of positive definite matrices, **A** and **B**, [5]

$$\mathbf{A} \preceq \mathbf{B} \iff \mathbf{A}^{-1} \succcurlyeq \mathbf{B}^{-1}. \quad \blacksquare$$

Lemma 8 Let $K_1, K_2 \subseteq \mathbb{R}^n$ be two convex sets with twice continuously differentiable (\mathcal{C}^2) boundary.

If $K_1 \supseteq K_2$, then the Jacobians $\mathbf{J}_{\Pi_{K_1}}(x)$ and $\mathbf{J}_{\Pi_{K_2}}(x)$ of metric projections onto K_1 and K_2 , respectively, satisfy

$$\mathbf{J}_{\Pi_{K_1}}(x) \succcurlyeq \mathbf{J}_{\Pi_{K_2}}(x), \quad (92)$$

for all $x \in \mathbb{R}^n \setminus K_1$ with $\Pi_{K_1}(x) = \Pi_{K_2}(x)$.

Proof: For any $x \in \mathbb{R}^n \setminus K_1$ with $\Pi_{K_1}(x) = \Pi_{K_2}(x)$ and $y \in \mathbb{R}^n$, one can write the metric projection of $x+y$ onto K_1 and K_2 , respectively, as

$$\Pi_{K_1}(x+y) = \Pi_{K_1}(x) + \mathbf{J}_{\Pi_{K_1}}(x)y + o(y), \quad (93a)$$

$$\Pi_{K_2}(x+y) = \Pi_{K_2}(x) + \mathbf{J}_{\Pi_{K_2}}(x)y + o(y), \quad (93b)$$

where $\lim_{\|y\| \rightarrow 0} \frac{o(y)}{\|y\|} = 0$. Further, since $K_1 \supseteq K_2$, by the monotonicity of metric projections, we have

$$\|x+y - \Pi_{K_1}(x+y)\|^2 \leq \|x+y - \Pi_{K_2}(x+y)\|^2. \quad (94)$$

Now it follows from (93), (94) and Lemma 5 that

$$\begin{aligned} & \frac{\|(I - \mathbf{J}_{\Pi_{K_2}}(x))y\|^2}{\|y\|^2} - \frac{\|(I - \mathbf{J}_{\Pi_{K_1}}(x))y\|^2}{\|y\|^2} \geq \\ & \frac{\|x - \Pi_{K_1}(x) - o(y)\|^2}{\|y\|^2} - \frac{\|x - \Pi_{K_2}(x) - o(y)\|^2}{\|y\|^2} \\ & + \frac{2y^T(\mathbf{J}_{\Pi_{K_1}}(x) - \mathbf{J}_{\Pi_{K_2}}(x))o(y)}{\|y\|^2}, \quad (95) \end{aligned}$$

where the right hand side converges to zero as $\|y\| \rightarrow 0$. Therefore, for any $y \in \mathbb{R}^n$, one always has

$$\|(I - \mathbf{J}_{\Pi_{K_2}}(x))y\|^2 \geq \|(I - \mathbf{J}_{\Pi_{K_1}}(x))y\|^2. \quad (96)$$

Thus, the result follows since $\mathbf{0} \preceq \mathbf{J}_{\Pi_{K_1}}(x), \mathbf{J}_{\Pi_{K_2}}(x) \preceq \mathbf{I}$ (Lemma 5). \blacksquare

APPENDIX V CONVEXITY IN POLAR COORDINATES

Similar to the notion of convexity in Cartesian coordinates, a polar curve $\rho : (\theta_l, \theta_u) \rightarrow \mathbb{R}_{\geq 0}$ is said to be

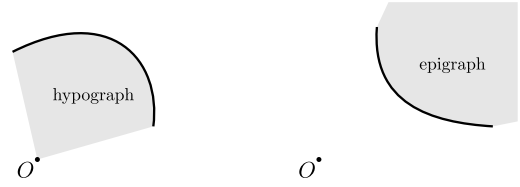


Fig. 6. Convexity in polar coordinates. A polar curve is convex (concave) with respect to the pole iff its epigraph (hypograph) is a convex set, as illustrated on the right (left, respectively).

convex with respect to the pole if and only if its epigraph,²² $\text{epi}\rho := \{(\theta, \varrho) | \theta \in (\theta_l, \theta_u), \varrho \geq \rho(\theta)\}$, is a convex set; and, likewise, ρ is said to be *concave* if and only if its hypograph, $\text{hyp}\rho := \{(\theta, \varrho) | \theta \in (\theta_l, \theta_u), 0 \leq \varrho \leq \rho(\theta)\}$ is a convex set [17, 37], see Fig. 6.

Alternatively, like the first- and second-order conditions for convexity of Cartesian functions, one can verify the convexity of a polar curve as follows:

Theorem 4 (Second-Order Convexity Condition [37]) A twice differentiable polar curve $\rho : (\theta_l, \theta_u) \rightarrow \mathbb{R}_{>0}$ is said to be convex with respect to the pole if²³

$$\Gamma := \rho^2 + 2\left(\frac{d\rho}{d\theta}\right)^2 - \rho\frac{d^2\rho}{d\theta^2} \leq 0. \quad (99)$$

Theorem 5 (Three-Point Convexity Condition [17]) A polar curve $\rho : (\theta_l, \theta_u) \rightarrow \mathbb{R}_{>0}$ is convex to the pole if²⁴

$$\det\left(\begin{bmatrix} \frac{1}{\rho(\theta_1)} & \cos \theta_1 & \sin \theta_1 \\ \frac{1}{\rho(\theta_2)} & \cos \theta_2 & \sin \theta_2 \\ \frac{1}{\rho(\theta_3)} & \cos \theta_3 & \sin \theta_3 \end{bmatrix}\right) \cdot \det\left(\begin{bmatrix} 1 & \cos \theta_1 & \sin \theta_1 \\ 1 & \cos \theta_2 & \sin \theta_2 \\ 1 & \cos \theta_3 & \sin \theta_3 \end{bmatrix}\right) \leq 0, \quad (100)$$

for all $\theta_1, \theta_2, \theta_3 \in (\theta_l, \theta_u)$.

²²Note that here the epigraph and the hypograph of a polar curve are given in polar coordinates, and one can equivalently write them in Cartesian coordinates as

$$\text{epi}\rho = \{(\varrho \cos \theta, \varrho \sin \theta) | \theta \in (\theta_l, \theta_u), \varrho \geq \rho(\theta)\}, \quad (97)$$

$$\text{hyp}\rho = \{(\varrho \cos \theta, \varrho \sin \theta) | \theta \in (\theta_l, \theta_u), 0 \leq \varrho \leq \rho(\theta)\}. \quad (98)$$

²³In [37], the convexity of a polar curve with respect to the pole is characterized based on its tangent lines: a polar curve at a point is convex iff the curve in a small neighborhood of that point lies on the opposite side of the tangent at that point to the pole. Accordingly, the second-order convexity condition in (99) is derived using the perpendicular distance p of the pole to the tangent line of a polar curve ρ at point $(\theta, \rho(\theta))$, given by

$$\frac{1}{p^2} = u^2 + \left(\frac{du}{d\theta}\right)^2, \quad (101)$$

where $u := \frac{1}{\rho}$; and the polar curve ρ is said to be convex to the pole if and only if $\frac{dp}{d\theta}$ is negative, where

$$\frac{dp}{d\theta} = p^3 u^2 \left(u + \frac{d^2 u}{d\theta^2}\right) = \frac{p^3}{\rho^2} \left(\rho^2 + 2\left(\frac{d\rho}{d\theta}\right)^2 - \rho\frac{d^2\rho}{d\theta^2}\right). \quad (102)$$

²⁴Let $\mathbf{v}_t = (\cos \theta_t, \sin \theta_t)$ and $\mathbf{p}_t = (\rho(\theta_t) \cos \theta_t, \rho(\theta_t) \sin \theta_t)$ for $t = 1, 2, 3$. Then, to have a geometric understanding of the three-point convexity condition one can equivalently rewrite (100) as

$$((\mathbf{p}_2 - \mathbf{p}_1) \times (\mathbf{p}_3 - \mathbf{p}_2)) \cdot ((\mathbf{v}_2 - \mathbf{v}_1) \times (\mathbf{v}_3 - \mathbf{v}_2)) \leq 0, \quad (103)$$

where \times and \cdot denote the cross and dot products, respectively.

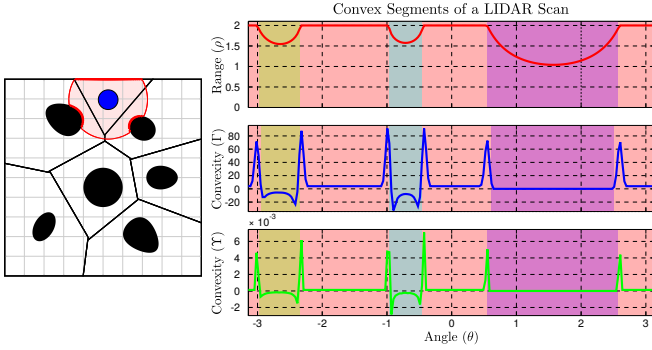


Fig. 7. Segmentation of a LIDAR scan into convex polar curves using convexity measures Γ (99) and Υ (100).^{25 26}

Note that the second determinant term in (100) quantifies the circular order of θ_1 , θ_2 and θ_3 , i.e., it is positive (negative) if these angles are given in counter-clockwise (clockwise, respectively) order.

In accordance with Theorem 5, since a LIDAR scanner has a fixed angular resolution in practice, say $\Delta\theta \in (0, \pi)$, to check the convexity of a LIDAR scan in counter-clockwise angular order, we find it convenient to define

$$\Upsilon(\theta) := \det \begin{pmatrix} \frac{1}{\rho(\theta - \Delta\theta)} & \cos(\theta - \Delta\theta) & \sin(\theta + \Delta\theta) \\ \frac{1}{\rho(\theta)} & \cos(\theta) & \sin(\theta) \\ \frac{1}{\rho(\theta + \Delta\theta)} & \cos(\theta + \Delta\theta) & \sin(\theta + \Delta\theta) \end{pmatrix}. \quad (104)$$

Therefore one can identify the convex polar curve segments of a LIDAR scan using the convexity measures Γ (99) and Υ (104) as illustrated in Fig. 7.

APPENDIX VI

AN EXTENSION FOR A DISCRETE-TIME ROBOT MODEL

Keeping in mind its potential application to online robot navigation in a nonconvex environment when combined with a standard (e.g., sampling based) motion planning algorithm — a future research direction we will explore in a subsequent paper, we now introduce a discrete-time version of the “move-to-projected-goal” law in (10) to iteratively navigate towards a designated goal location $x^* \in \mathcal{F}$ as follows: for any $x^k \in \mathcal{F}$,

$$x^{k+1} = x^k - (x^k - \Pi_{\mathcal{L}\mathcal{F}(x^k)}(x^*))\Delta t, \quad (105)$$

where $k \in \mathbb{N}$ is a discrete time index, $\Delta t \in (0, 1]$ is a fixed sample time (step size), and $\Pi_{\mathcal{L}\mathcal{F}(x^k)}(x^*)$ (4) is the metric projection of the goal x^* onto the robot’s local free space $\mathcal{L}\mathcal{F}(x^k)$ (9). Note that we here avoid collisions along the line segment joining consecutive robot states, x^k and x^{k+1} , by limiting the range of values of Δt to $(0, 1]$ since x^{k+1} becomes a convex combination of the robot state x^k and the projected

²⁵ Here, we set the LIDAR’s angular resolution to $\Delta\theta = \frac{\pi}{100}$, and approximately compute the first- and second-order derivatives of a simulated LIDAR range data, respectively, using its three-point first- and second-order central differences [20] after smoothing with a five-point Gaussian moving average filter with unit variance, $\sigma^2 = 1$ [49].

²⁶ A practical heuristic for identifying convex segments of a LIDAR scan is its segmentation based on local maxima; however, such a heuristic approach might detect some concave curve segments in addition to all convex segments in a LIDAR scan.

goal $\Pi_{\mathcal{L}\mathcal{F}(x^k)}(x^*)$, i.e., $x^{k+1} = (1 - \Delta t)x^k + \Delta t \Pi_{\mathcal{L}\mathcal{F}(x^k)}(x^*)$, and the line segment joining them is always free of collisions (Corollary 1).

Therefore, using the continuity of the move-to-projected-goal law in (10) (Proposition 2) and the type of its stationary points (Proposition 6), one can conclude that:

Corollary 4 *If Assumption 2 holds for the goal and for all obstacles, then the discrete-time “move-to-projected-goal” law in (105) starting from almost any robot location in \mathcal{F} (1) iteratively reaches a small neighborhood, $B(x^*, \epsilon)$ for some $\epsilon > 0$, of the goal x^* in finite steps with the guarantee of no collisions along the line segments joining two consecutive robot states, while strictly decreasing the Euclidean distance to the goal.*

Note that the discrete-time “move-to-projected-goal” law in (105) can be simply adapted to limited range sensing models, by using the robot’s sensed local free space $\mathcal{L}\mathcal{F}_S$ (24) or the line-of-sight local free space $\mathcal{L}\mathcal{F}_L$ (30), as well as to the differential drive model while retaining the convergence and collision avoidance guarantees.

To demonstrate its motion pattern, we present in Fig. 8 the resulting navigation paths of the discrete-time “move-to-projected-goal” law in (105) for different sampling times and sensing models.

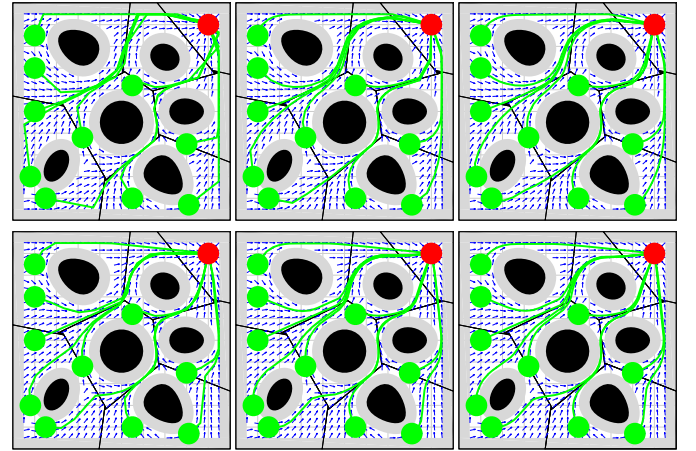


Fig. 8. Example navigation paths of the discrete-time “move-to-projected-goal” law for different sampling times and sensing models: (left) $\Delta t = 1$, (middle) $\Delta t = 0.5$, and (right) $\Delta t = 0.25$; and (top) local Voronoi-adjacent¹⁰ obstacle sensing, and (bottom) a fixed radius sensory footprint.

APPENDIX VII

MOTION PATTERN FAR AWAY FROM THE GOAL

In Fig. 9 we present the motion pattern generated by the “move-to-projected-goal” law starting at a set of initial robot configurations far away from the goal, located at the upper right corner of a 50×10 environment populated with convex obstacles, for different sensing and actuation models.

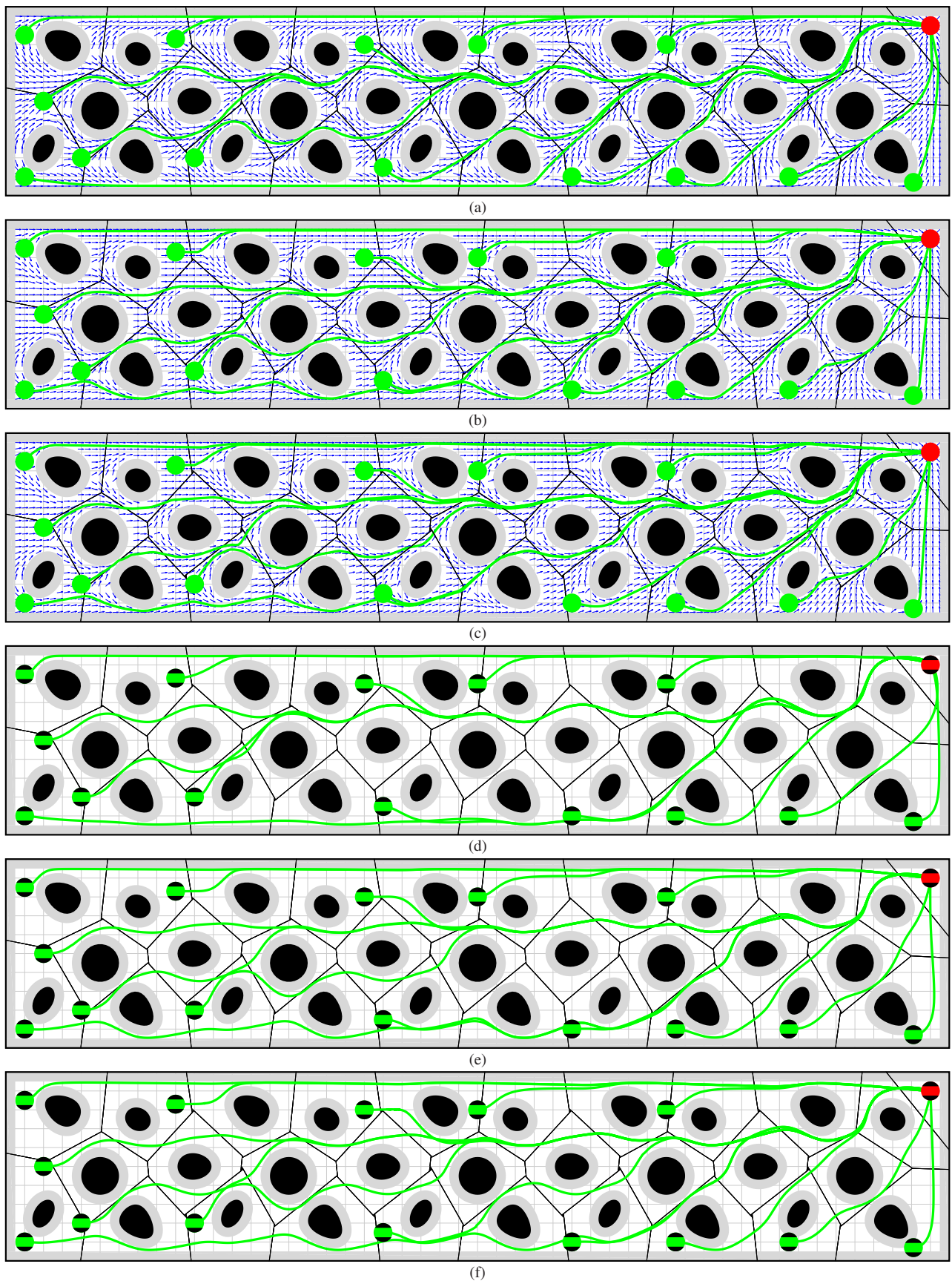


Fig. 9. Example navigation trajectories of the “move-to-projected-goal” law starting at a set of initial conditions (green) far away from the goal (red) for different sensing and actuation models: (a,b,c) a fully actuated robot, (d,e,f) a differential drive robot, (a,d) local Voronoi-adjacent¹⁰ obstacle sensing, (b,e) a fixed radius sensory footprint, (c,f) a limited range line-of-sight sensor.

REFERENCES

- [1] Omur Arslan and Daniel E. Koditschek. Voronoi-based coverage control of heterogeneous disk-shaped robots. In *Robotics and Automation, 2016 IEEE International Conference on*, 2016.
- [2] Omur Arslan and Daniel E. Koditschek. Exact robot navigation using power diagrams. In *Robotics and Automation, 2016 IEEE International Conference on*, 2016.
- [3] Alessandro Astolfi. Exponential stabilization of a wheeled mobile robot via discontinuous control. *Journal of Dynamic Systems, Measurement, and Control*, 121(1): 121–126, 1999.
- [4] Franz Aurenhammer. Power diagrams: Properties, algorithms and applications. *SIAM Journal on Computing*, 16(1):78–96, 1987.
- [5] Rajendra Bhatia. *Positive Definite Matrices*. Princeton Series in Applied Mathematics. Princeton University Press, 2007.
- [6] Stephen Boyd and Lieven Vandenberghe. *Convex Optimization*. Cambridge University Press, 2004.
- [7] Roger W. Brockett. *Asymptotic stability and feedback stabilization*. Defense Technical Information Center, 1983.
- [8] Francesco Bullo, Jorge Cortés, and Sonia Martinez. *Distributed Control of Robotic Networks: A Mathematical Approach to Motion Coordination Algorithms*. Princeton University Press, 2009.
- [9] Robert R. Burridge, Alfred A. Rizzi, and Daniel E. Koditschek. Sequential composition of dynamically dexterous robot behaviors. *The International Journal of Robotics Research*, 18(6):535–555, 1999.
- [10] Robin W. Chaney. Piecewise ck functions in nonsmooth analysis. *Nonlinear Analysis: Theory, Methods & Applications*, 15(7):649 – 660, 1990.
- [11] Howie Choset and Joel Burdick. Sensor-based exploration: The hierarchical generalized voronoi graph. *The International Journal of Robotics Research*, 19(2):96–125, 2000.
- [12] Howie Choset, Kevin M. Lynch, Seth Hutchinson, George A. Kantor, Wolfram Burgard, Lydia E. Kavraki, and Sebastian Thrun. *Principles of Robot Motion: Theory, Algorithms, and Implementations*. MIT Press, Cambridge, MA, 2005.
- [13] David C. Conner, Howie Choset, and Alfred A. Rizzi. Flow-through policies for hybrid controller synthesis applied to fully actuated systems. *Robotics, IEEE Transactions on*, 25(1):136–146, 2009.
- [14] David C. Conner, Howie Choset, and Alfred A. Rizzi. Integrating planning and control for single-bodied wheeled mobile robots. *Autonomous Robots*, 30(3):243–264, 2011.
- [15] Christopher I. Connolly and Roderic A. Grupen. The applications of harmonic functions to robotics. *Journal of Robotic Systems*, 10(7):931–946, 1993.
- [16] Jorge Cortés, Sonia Martinez, Timur Karatas, and Francesco Bullo. Coverage control for mobile sensing networks. *Robotics and Automation, IEEE Transactions on*, 20(2):243–255, 2004.
- [17] Harold G. Eggleston. *Convexity*. Cambridge University Press, 1958.
- [18] Ioannis Filippidis and Kostas J. Kyriakopoulos. Adjustable navigation functions for unknown sphere worlds. In *Decision and Control and European Control Conference (CDC-ECC), 2011 50th IEEE Conference on*, pages 4276–4281, 2011.
- [19] Simon Fitzpatrick and Robert R. Phelps. Differentiability of the metric projection in Hilbert space. *Transactions of the American Mathematical Society*, 270(2):483–501, 1982.
- [20] Bengt Fornberg. Generation of finite difference formulas on arbitrarily spaced grids. *Mathematics of Computation*, 51(184):699–706, 1988.
- [21] Robert M. Haralick, Stanley R. Sternberg, and Xinhua Zhuang. Image analysis using mathematical morphology. *Pattern Analysis and Machine Intelligence, IEEE Transactions on*, 9(4):532–550, 1987.
- [22] Peter Henry, Christian Vollmer, Brian Ferris, and Dieter Fox. Learning to navigate through crowded environments. In *Robotics and Automation (ICRA), 2010 IEEE International Conference on*, pages 981–986, 2010.
- [23] Morris W. Hirsch, Stephen Smale, and Robert L. Devaney. *Differential Equations, Dynamical Systems, and an Introduction to Chaos*. Academic press, 2nd edition, 2003.
- [24] Richard B. Holmes. Smoothness of certain metric projections on Hilbert space. *Transactions of the American Mathematical Society*, 184:87–100, 1973.
- [25] Aaron M. Johnson, Matthew T. Hale, Galen C. Haynes, and Daniel E. Koditschek. Autonomous legged hill and stairwell ascent. In *Safety, Security, and Rescue Robotics (SSRR), 2011 IEEE International Symposium on*, pages 134–142, 2011.
- [26] Sertac Karaman and Emilio Frazzoli. High-speed flight in an ergodic forest. In *Robotics and Automation (ICRA), 2012 IEEE International Conference on*, pages 2899–2906, 2012.
- [27] Hassan K. Khalil. *Nonlinear Systems*. Prentice Hall, 3rd edition, 2001.
- [28] Oussama Khatib. Real-time obstacle avoidance for manipulators and mobile robots. *The International Journal of Robotics Research*, 5(1):90–98, 1986.
- [29] Daniel E. Koditschek. Exact robot navigation by means of potential functions: Some topological considerations. In *Robotics and Automation. Proceedings. 1987 IEEE International Conference on*, volume 4, pages 1–6, 1987.
- [30] Daniel E. Koditschek and Elon Rimon. Robot navigation functions on manifolds with boundary. *Advances in Applied Mathematics*, 11(4):412 – 442, 1990.
- [31] M.K. Kozlov, S.P. Tarasov, and L.G. Khachiyan. The polynomial solvability of convex quadratic programming.

- USSR Computational Mathematics and Mathematical Physics*, 20(5):223–228, 1980.
- [32] Ludwig Kuntz and Stefan Scholtes. Structural analysis of nonsmooth mappings, inverse functions, and metric projections. *Journal of Math. Analysis and Applications*, 188(2):346–386, 1994.
- [33] Andrew Kwok and Sonia Martnez. Deployment algorithms for a power-constrained mobile sensor network. *International Journal of Robust and Nonlinear Control*, 20(7):745–763, 2010.
- [34] Steven M. LaValle. *Planning Algorithms*. Cambridge University Press, Cambridge, U.K., 2006.
- [35] Grigoris Lionis, Xanthi Papageorgiou, and Kostas J. Kyriakopoulos. Locally computable navigation functions for sphere worlds. In *Robotics and Automation, 2007 IEEE International Conference on*, pages 1998–2003, 2007.
- [36] Jiming Liu. Sensitivity analysis in nonlinear programs and variational inequalities via continuous selections. *SIAM Journal on Control and Optimization*, 33(4):1040–1060, 1995.
- [37] James McMahon and Virgil Snyder. *Elements of the Differential Calculus*. American Book Company, 1898.
- [38] James Munkres. *Topology*. Pearson, 2nd edition, 2000.
- [39] Colm Ó’Dúnlaing and Chee K. Yap. A retraction method for planning the motion of a disc. *Journal of Algorithms*, 6(1):104 – 111, 1985.
- [40] Atsuyuki Okabe, Barry Boots, Kokichi Sugihara, and Sung Nok Chiu. *Spatial tessellations: concepts and applications of Voronoi diagrams*, volume 501. John Wiley & Sons, 2nd edition, 2000.
- [41] Aditya A. Paranjape, Kevin C. Meier, Xichen Shi, Soon-Jo Chung, and Seth Hutchinson. Motion primitives and 3D path planning for fast flight through a forest. *The International Journal of Robotics Research*, 34(3):357–377, 2015.
- [42] Santiago Paternain, Daniel E. Koditschek, and Alejandro Ribeiro. Navigation functions for convex potentials in a space with convex obstacles. *IEEE Transactions on Automatic Control*, (submitted).
- [43] Kaare Brandt Petersen and Michael Syskind Pedersen. *The Matrix Cookbook*. Technical University of Denmark, 2012.
- [44] Luciano C.A. Pimenta, Vijay Kumar, Renato C. Mesquita, and Guilherme A.S. Pereira. Sensing and coverage for a network of heterogeneous robots. In *Decision and Control, IEEE Conference on*, pages 3947–3952, 2008.
- [45] Elon Rimon and Daniel E. Koditschek. Exact robot navigation using artificial potential functions. *Robotics and Automation, IEEE Transactions on*, 8(5):501–518, 1992.
- [46] R.Tyrrell Rockafellar. Lipschitzian properties of multifunctions. *Nonlinear Analysis: Theory, Methods & Applications*, 9(8):867–885, 1985.
- [47] Alexander Shapiro. Sensitivity analysis of nonlinear programs and differentiability properties of metric projections. *SIAM Journal on Control and Optimization*, 26(3):628–645, 1988.
- [48] James Stewart. *Calculus: Early Transcendentals*. Cengage Learning, 7th edition, 2012.
- [49] Richard Szeliski. *Computer Vision: Algorithms and Applications*. Springer, 2011.
- [50] Pete Trautman, Jeremy Ma, Richard M. Murray, and Andreas Krause. Robot navigation in dense human crowds: Statistical models and experimental studies of humanrobot cooperation. *The International Journal of Robotics Research*, 34(3):335–356, 2015.
- [51] Roger Webster. *Convexity*. Oxford University Press, 1995.
- [52] David Wooden, Matthew Malchano, Kevin Blankespoor, Andrew Howardy, Alfred A. Rizzi, and Marc Raibert. Autonomous navigation for BigDog. In *Robotics and Automation (ICRA), 2010 IEEE International Conference on*, pages 4736–4741, 2010.